

AD-A223 060

DTIC FILE COPY

2

# Velocity Selection to Enable Direct Measurement of Strong Single Atom - Optical Cavity Coupling

by

Michael E. Donovan

B.S. United States Military Academy  
(1981)

Submitted to the Department of Physics  
in partial fulfillment of the requirements for the degree of  
Master of Science in Physics

at the

MASSACHUSETTS INSTITUTE OF TECHNOLOGY

June 1990

© Massachusetts Institute of Technology 1990

Signature of Author ..... *Michael E. Donovan* .....

Department of Physics  
June 4, 1990

**DTIC**  
**ELECTE**  
**JUN 20 1990**  
*lo* **D**

Certified by .....

Michael S. Feld  
Professor of Physics  
Thesis Supervisor

Accepted by .....

George F. Koster  
Chairman, Departmental Committee on Graduate Students

**DISTRIBUTION STATEMENT A**  
Approved for public release  
Distribution Unlimited

90 06 19 027

# REPORT DOCUMENTATION PAGE

Form Approved  
OMB No. 0704-0188

Public reporting burden for this collection of information is estimated to average 1 hour per response, including the time for reviewing instructions, searching existing data sources, gathering and maintaining the data needed, and reviewing the collection of information. Send comments regarding this burden estimate or any other aspect of this collection of information, including suggestions for reducing this burden, to Washington Headquarters Services, Directorate for Information Operations and Reports, 1215 Jefferson Davis Highway, Suite 1204, Arlington, VA 22202-4302, and to the Office of Information and Regulatory Affairs, Office of Management and Budget, Washington, DC 20503.

1. AGENCY USE ONLY (Leave Blank)		2. REPORT DATE 4 Jun 90	3. REPORT TYPE AND DATES COVERED Final	
4. TITLE AND SUBTITLE Direct Velocity Selection to Enable Measurement of Strong Single Atom Optical Cavity Coupling			5. FUNDING NUMBERS Civil Schooling, AR621-1	
6. AUTHOR(S) CPT Michael E. Donovan				
7. PERFORMING ORGANIZATION NAME(S) AND ADDRESS(ES) Spectroscopy Laboratory Massachusetts Institute of Technology Cambridge, MA 02139			8. PERFORMING ORGANIZATION REPORT NUMBER	
9. SPONSORING/MONITORING AGENCY NAME(S) AND ADDRESS(ES) Fully funded civil schooling under AR 621-1 sponsored by US Army			10. SPONSORING/MONITORING AGENCY REPORT NUMBER	
11. SUPPLEMENTARY NOTES Prepared in partial fulfillment of the requirements for the Master of Science Degree in Physics at Massachusetts Institute of Technology				
12a. DISTRIBUTION/AVAILABILITY STATEMENT Available to the general public Copyright to MIT			12b. DISTRIBUTION CODE	
13. ABSTRACT (Maximum 200 words) This thesis evaluates whether a velocity selector can sufficiently reduce Doppler broadening of a concentric optical cavity coupled to single atoms in an atomic beam so that the normal mode splitting can be observed. A simplified model of the atom-cavity system as undamped coupled oscillators is used to derive the coupling strength. The theory of velocity selectors is reviewed and a density reduction formula is derived and studied. Considerations for building a velocity selector for an atom-cavity experiment are examined. A tentative inclusion of cavity Doppler broadening in a semi-classical theory is presented. Experiments are presented which show good agreement to theory for density reduction at high velocity selector speeds and an additional density loss of 50% when selecting atoms less than 20% of thermal velocity. Data shows both effusive and supersonic beams,				
14. SUBJECT TERMS Optical Cavity Coupling, Physics (JG) Cavity Q.E.D., Velocity Selector, Doppler broadening, Thesis, Electromagnetism, Papers, Spectroscopy, Single Atom			15. NUMBER OF PAGES 89	
17. SECURITY CLASSIFICATION OF REPORT Unclass			18. PRICE CODE	
18. SECURITY CLASSIFICATION OF THIS PAGE Unclass		19. SECURITY CLASSIFICATION OF ABSTRACT Unclass		20. LIMITATION OF ABSTRACT UL

# Velocity Selection to Enable Direct Measurement of Strong Single Atom - Optical Cavity Coupling

by

Michael E. Donovan

Submitted to the Department of Physics  
on June 4, 1990, in partial fulfillment of the  
requirements for the degree of  
Master of Science in Physics

## Abstract

This thesis evaluates whether a velocity selector can sufficiently reduce Doppler broadening of a concentric optical cavity coupled to single atoms in an atomic beam so that the normal mode splitting can be observed. A simplified model of the atom-cavity system as undamped coupled oscillators is used to derive the coupling strength. The theory of velocity selectors is reviewed and a density reduction formula is derived and studied. Considerations for building a velocity selector for an atom-cavity experiment are examined. A tentative inclusion of cavity Doppler broadening in a semi-classical theory is presented.

Experiments are presented which show good agreement to theory for density reduction at high velocity selector speeds and an additional density loss of 50% when selecting atoms less than 20% of thermal velocity. Data shows both effusive and supersonic beams.

Providing our theory adequately models the cavity Doppler effect, velocity selection is shown to provide adequate velocity profiles and atomic densities to resolve the normal mode splitting with the velocity selector used in this thesis. This velocity selector has an unusually broad resolution and the splitting should be resolvable if it selects atoms with an average speed of around fifteen percent of thermal velocity (which is about 6000 cm/sec).

Thesis Supervisor: Michael S. Feld  
Title: Professor of Physics



Accession For	
NTIS - CB&I	<input checked="" type="checkbox"/>
DTIC - TAB	<input type="checkbox"/>
Unannounced	<input type="checkbox"/>
Justification	
By	
Distribution	
Availability Codes	
Dist	Availability or Special
A-1	

## Acknowledgments

I wish to thank the Army for its wealth of challenges in the last nine years, this certainly being one of them. I wish to thank Joe Mackin for selling this research opportunity and providing unlimited assistance. I wish to thank Michael Feld for hiring me and providing moral support.

The burden of making me into an experimentalist fell on Jim Childs and most of what is in this thesis must be ultimately credited to him. Kyungwon An has been selfless, especially in helping me with the computer work.

I will have fond memories of Tim Hutton, Bill Dalby, Ramchandra Dasari, and a host of others who lent me their expertise or just their friendship on many occasions. If I tried to list them all, I would inevitably fail.

I have fallen far short of spending the time I promised with my wife and children, having far underestimated the demands of this experiment. For them I have what I hope is a more realistic promise to spend more time together at West Point.

# Contents

<b>1</b>	<b>Introduction</b>	<b>6</b>
1.1	Atom-Cavity Experiments . . . . .	6
1.2	Two Approaches to Single Atom - Optical Cavity Splitting . . . . .	9
1.3	Experimental Measurement of Cavity Broadening Without Velocity Selection	11
1.4	Options to Achieve a Slow Atom Distribution . . . . .	13
1.5	Thesis Organization . . . . .	14
<b>2</b>	<b>Basic Theory of Normal Mode Splitting</b>	<b>16</b>
2.1	Simple Coupled Oscillator Model . . . . .	16
2.2	Experimental Realization of Atom-Cavity Coupled Oscillators . . . . .	20
2.3	More Complete Semiclassical Theory and Splitting Conditions . . . . .	22
2.4	The Splitting Condition in Terms Of Cavity Parameters . . . . .	24
<b>3</b>	<b>Velocity Selector Theory</b>	<b>26</b>
3.1	General Theory of Operation . . . . .	26
3.2	Density Reduction . . . . .	28
3.2.1	Beam Divergence . . . . .	29
3.2.2	Velocity Selection Density Reduction . . . . .	30
3.3	Velocity Selector Design . . . . .	32
3.3.1	Selection of Resolution . . . . .	32
3.3.2	Construction of Velocity Selector . . . . .	35

<b>4</b>	<b>Cavity Doppler Effect Theory</b>	<b>42</b>
4.1	The Cavity Doppler Effect . . . . .	42
4.2	Modified Semiclassical Equations . . . . .	44
4.2.1	Atom-Cavity Emission Lineshape . . . . .	45
4.3	Doppler Reduced Coupling . . . . .	46
4.4	Computer Solution to Doppler Modified Lineshape . . . . .	48
4.5	Computer Generated Lineshapes . . . . .	49
<b>5</b>	<b>Velocity Selection Experiments</b>	<b>55</b>
5.1	Objectives . . . . .	55
5.2	Conduct of the Experiments . . . . .	57
5.2.1	Interpreting the Data . . . . .	59
5.2.2	Controlling the Environment . . . . .	60
5.3	Fitting Doppler Profiles . . . . .	62
5.3.1	Unselected Profiles . . . . .	62
5.3.2	Misalignment . . . . .	68
5.3.3	Selected Profiles . . . . .	70
5.4	Density Reduction . . . . .	70
5.5	Error Analysis . . . . .	73
5.6	Absolute Density Estimate . . . . .	74
5.7	Recommendations and Conclusions . . . . .	75
<b>A</b>	<b>Flowchart for Computing Atom-Cavity System Lineshape</b>	<b>77</b>
<b>B</b>	<b>Optimization of Counting Time</b>	<b>84</b>

# Chapter 1

## Introduction

This thesis is part of a larger experiment to directly measure for the first time the normal mode frequency splitting of a single two-level atom strongly coupled to an optical cavity. It examines the use of a mechanical velocity selector to reduce Doppler broadening of the cavity resonance, which has to date kept us from resolving the splitting.

### 1.1 Atom-Cavity Experiments

By observing an excited two-level atom in a cavity which in some way alters the vacuum electric field, we hope to better understand the interaction of the vacuum with matter. In elementary quantum mechanics, an atom in an energy eigenstate has no probability of decay if left unperturbed. Thus considered, the phenomenon of spontaneous emission of an atom in free space is paradoxical. It is only with the quantization of the electric field as an ensemble of harmonic oscillators with finite ground state energies that we can understand spontaneous emission as an electric dipole interaction. Quantum electrodynamics provides a framework in which we understand the vacuum not as empty space, but as a space in which the ground state electromagnetic field arises from random fluctuations.

The semi-classical formalism in which electromagnetism is treated classically would

seem not to apply to effects which arise from vacuum field fluctuations, but, surprisingly, it does predict the same emission spectrum as fully quantum electrodynamical treatments. Using semi-classical theory, the single atom and optical resonator system reduces to two coupled oscillators, and the phenomena we associate with coupled mechanical oscillators can be easily associated with properties of the atom-cavity system. For coupled oscillators which share a single resonant frequency, we see an exchange of energy at a rate equal to half the frequency difference of the two normal modes, provided the coupling is not too strong and damping can be neglected [1][pp. 106-107]. This energy exchange rate, or frequency splitting, is a measure of the coupling strength.

Experiments exploring this coupling rate or normal mode splitting have been performed previously, and have exhibited the predicted results, but they differ from our experiment in some important respects. Since microwave cavities can have very high  $Q$ , the desired experimental conditions are more easily achieved, and measurements of the single atom energy exchange rate have been indirectly made by counting Rydberg atoms left in the excited state [2][p. 27]. Optical regime experiments, on the other hand, make measurements by directly counting visible photons and should exhibit better signal to noise ratios, making the single atom and optical cavity system a more precise tool for studying the atom-field interaction. Jeffrey Kimble and his colleagues have studied atom-cavity coupling using visible wavelength radiation, but their experiments were unable to resolve the single atom splitting [3][pp. 146-148]. It is important to note, however, that they did observe splitting for systems with as few as forty atoms, for which the coupling rate is enhanced by a factor of the square root of the number of atoms. In studying many atom systems, quantum effects may be masked by statistical fluctuations, so researchers ultimately desire to study the more elementary single atom and single cavity mode splitting [2][p. 30]. This goal has been a very difficult one to achieve from both a physics and an engineering perspective.

Our optical resonator, two concentric mirrors, enhances the atom-field coupling by focusing the vacuum electric field onto the atom at cavity center. Since this focusing is

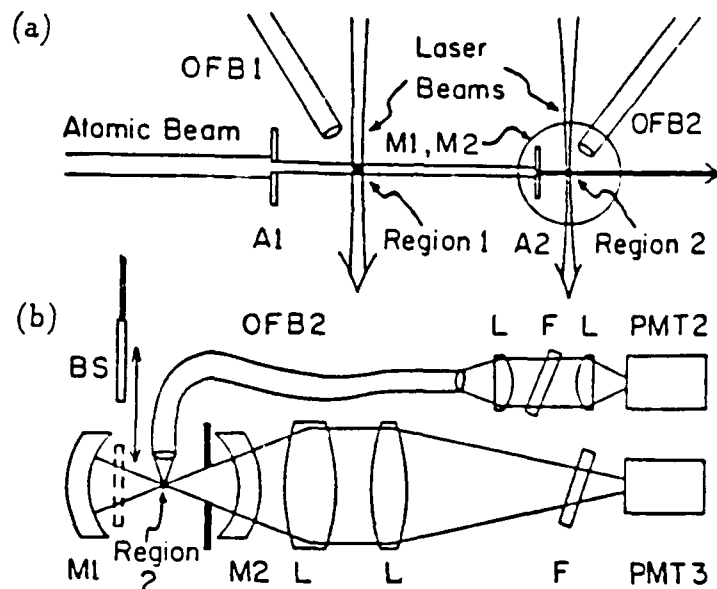


Figure 1-1: Atom-Cavity Coupling Experiment. (a) Relative orientation of the atomic beam, laser beams, apertures (A), cavity mirrors (M), and optical fiber bundles (OFB). Region 1 is the "free space" reference. Region 2 is the atom-cavity system. (b) Side view of the cavity showing the positions of the mirrors, lenses, interference filters (F), moveable beam stop (BS), optical fiber bundle 2, and two of the three photomultiplier tubes.

limited by diffraction, the coupling drops off as we decrease the solid angle subtended by the mirrors. In our experiments, barium atoms pass through the center of the cavity in a thermal beam at right angles to both the exciting laser and the cavity axis (see Figure 1.1[4]). Since the atoms have no velocity component in the direction of the exciting laser, there is no Doppler broadening in the usual sense. But the cavity sees photons spontaneously emitted by these atoms which *are* Doppler shifted unless they are emitted in the plane perpendicular to the atomic beam. At an angle  $\theta$  to this plane, a photon from an atom of velocity  $v$  is Doppler shifted by  $kv \sin \theta$ ; since the atoms have a broad distribution of velocities and emit photons over the entire solid angle subtended by the mirrors, we see a Doppler broadened atom-cavity system resonance in which the normal mode splitting is washed out. It is this effect we are trying to eliminate with the velocity selector.

## 1.2 Two Approaches to Single Atom - Optical Cavity Splitting

The particular manifestation of the Doppler effect described above would be unimportant if the solid angle from the atom subtended at the mirrors were made small enough. In the experiments of Kimble et al. this is indeed the case. To understand why we have not elected to follow a similar path, consider the condition for the strong coupling limit where the splitting exists for a cavity tuned to the atomic center frequency (derived in Chapter 2):

$$g > \gamma_c, \gamma_p$$

where  $2\gamma_p$  is the free space spontaneous emission rate,  $2\gamma_c$  is the cavity decay rate, and  $g$  is the atom-cavity coupling rate

$$g = \frac{\mu}{\hbar} \sqrt{\frac{2\pi\hbar\omega}{V}}$$

which is a function of the electric dipole moment  $\mu$ , free space atomic center frequency  $\omega$ , and the effective mode volume  $V$ . Once the atomic transition is selected,  $\gamma_p$  is fixed. Present mirror technology enables one to achieve a very small cavity linewidth,  $\gamma_c$ , with large radius of curvature mirrors. The coupling rate, however, is small for these large radius of curvature mirrors because the effective mode volume is relatively large compared to the lower finesse mirrors we have been using. The key to understanding the difference between Kimble's approach and our approach lies in how the mode volume increases.

Since both experiments study spontaneous emission at the center of an open, symmetric optical cavity, it is fair to describe the cavity mode in both cases by a Gaussian beam in a lens waveguide (see Figure 1.2). The larger the radius of curvature of the lenses (mirrors) for a fixed separation less than the focal length, the less the beam is focused between the lenses and the less the effective mode volume of the cavity is decreased. For Kimble's cavity, where the radius of curvature is much greater than the mirror separation,

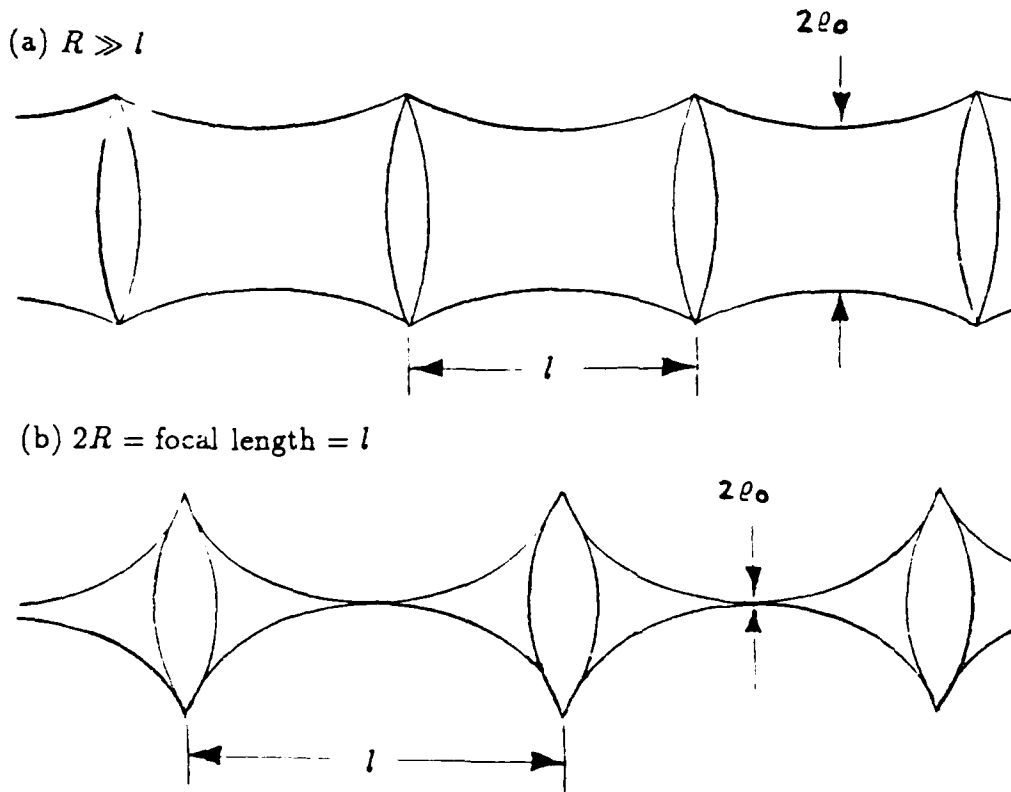


Figure 1-2: Lens Waveguides Equivalent in Ray Optics to Spherical Mirror Cavity

the cavity linewidth is small (about 1 MHz) [5][p. 249] and the effective mode volume is  $V = \int E^2(\vec{r}) d^3r / E_0^2 = \pi \rho_0^2 l$ , where  $\rho_0$  is the Gaussian beam spot radius at cavity center and  $l$  is the mirror separation.  $E(\vec{r})$  is the electric field amplitude, and  $E_0$  is that amplitude at the center of the cavity, which is also the atom position. Calculations done in Ammon Yariv's book *Quantum Electronics* show that for a chosen radius of curvature and mirror separation, the Gaussian beam waist, which is equivalent to our mode waist, is  $\rho_0 = \sqrt{\lambda z_0 / \pi}$ , where  $z_0^2 = (2R - l)l/4$ . [6][p.140] In these expressions,  $\lambda$  is the wavelength,  $R$  is the radius of curvature, and  $l$  is still the mirror separation; ray optics and the paraxial approximation are assumed. For  $R \gg l$ ,  $\rho_0$  approaches  $\sqrt[4]{\lambda^2 R l / 2\pi^2}$ , and it is this case which applies to Kimble's high finesse cavity.

In contrast, the cavity we use in our experiments is concentric, one of a class of degenerate resonators. The ray optics approximation cannot apply since it predicts the mode waist to vanish. Diffraction limits the beam waist to  $\rho_0 = \lambda / \pi \theta_{\text{beam}}$ , where  $\theta_{\text{beam}}$  is the angle the atom sees from the center to the edge of the mirrors. [6][p. 119] This case is very different! The mode volume decreases with increasing mirror diameter, which is now a variable parameter. The choice of this radius strongly affects the cavity linewidth

because of spherical aberration and microroughness, so in practice our goal is to fix the radius where both coupling and cavity linewidth are adequate. Since the coupling,  $g$ , is proportional to  $1/\sqrt{V}$ , the coupling in a concentric cavity is enhanced over the high finesse ordinary cavity by a factor:

$$\frac{g_{degenerate}}{g_{ordinary}} = \sqrt{\frac{V_{ordinary}}{V_{degenerate}}} = \sqrt{\frac{\pi \varrho_{0,ord}^2 l_{ord}}{\pi \varrho_{0,deg}^2 l_{deg}}} = \frac{\pi^{\frac{1}{2}} (R l_{ord})^{\frac{1}{4}} \theta_{beam}}{2^{\frac{1}{4}} \lambda^{\frac{1}{2}}} \sqrt{\frac{l_{ord}}{l_{deg}}}$$

Using typical numbers for the two experiments,  $R = 100\text{cm}$ ,  $l_{ord} = 0.1\text{cm}$ ,  $l_{deg} = 5\text{cm}$ ,  $\theta_{beam} = 0.2$ , and  $\lambda = 5 \times 10^{-5}\text{cm}$ , the coupling is enhanced by a factor of about eleven.

In order to exploit the advantages of a degenerate optical resonator, it is necessary that we use a larger solid angle than Kimble. In fact, we must find a solid angle small enough so it does not degrade cavity finesse too much due to mirror roughness, yet large enough so it does not make the effective mode volume too large. If the minimum solid angle that allows sufficient coupling exists with  $\gamma_c < g$ , then splitting should occur for that size pair of mirrors. We believe this can be achieved, provided the broadening from the Doppler effect can be made small enough.

### 1.3 Experimental Measurement of Cavity Broadening Without Velocity Selection

Before we took into account the cavity Doppler effect, we saw a much broader peak near the cavity resonance than we had expected. Figure 1.3 shows typical plots of transmitted fluorescence intensity through a cavity mirror as a function of pump laser frequency [7][p. 155]. The coupling rate for this experiment, estimated from fits to be 44 MHz, is smaller than the measured empty cavity linewidth of 160 MHz, so we do not expect any splitting at zero atom-cavity detuning for these mirrors (Figure 1.3a), but we do see peaks at both the atom and cavity resonances at large atom-cavity detuning (b and c). Since the coupling is weak at large detuning, the measured width of the cavity resonance peak

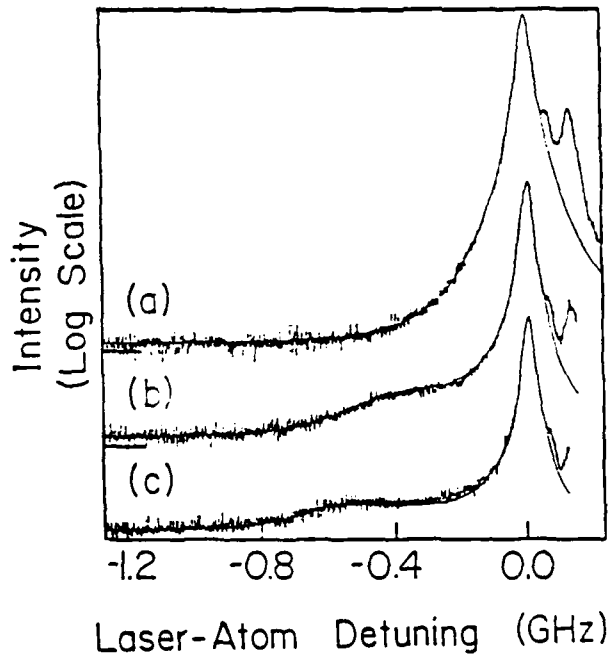


Figure 1-3: Observed fluorescence emitted through the mirrors. Plot (a) shows the cavity tuned to the atomic center frequency, plot (b) shows atom-cavity detuning of 475 MHz, and plot (c) shows atom-cavity detuning of 610 MHz

would be very nearly the empty cavity linewidth if it were not for the cavity Doppler effect. The empty cavity linewidth was experimentally determined by mode matching a TEM<sub>00</sub> laser beam into the cavity and measuring transmission as the cavity length was changed by applying a ramp voltage to piezoelectric transducer (PZT) stacks attached to one of the mirrors. Although the theoretical reflectivity limited cavity linewidth for these concentric spherical mirrors was about 60 MHz, we measured a broader empty cavity linewidth of 160 MHz primarily because of small mirror imperfections. This empty cavity measurement still accounts for only a fraction of the cavity linewidth we measure from the atom-cavity spectrum to be about 400 MHz, and we ascribe the difference to the cavity Doppler effect.

In the Doppler broadened limit, the cavity width should be on the order of  $2k\bar{v}\sin\theta_{max}$ , twice the absolute value of the maximum cavity Doppler shift of some "average" velocity atom. Taking this average velocity to be  $4 \times 10^4$  cm/sec, a typical

thermal velocity, and using a typical maximum cavity angle of .2, we get cavity Doppler broadening of around 300 MHz. This estimate should not be taken too seriously as it has ignored many complexities, but it does show why the data of Figure 1-3 has a cavity peak width more than twice the measured empty cavity linewidth of 160 MHz.

## 1.4 Options to Achieve a Slow Atom Distribution

Having established the need to reduce the cavity Doppler broadening to achieve adequate coupling, there remains the question of how to do so. Calculations from Chapter 4 show that we need an average atomic velocity of about 400 to 800 cm/sec, or 10 to 20 percent of thermal velocity to achieve an adequate  $\gamma_c$ . To achieve this, there are several options to consider, all with their respective costs in atomic density and/or time.

Before reviewing the options, let us first consider the effect of losing atomic beam density. Although there is an average of less than one atom in the cavity mode at any given time, the measured signal is a collection of photon counts from many atoms as the laser is tuned through the resonances of the atom-cavity system. The fluorescence is proportional to atomic density and exciting laser power. There is a limit to the laser power that can be used without saturating, and thus broadening, the atoms. There is also a limit to the density of atoms coming from the oven, which could be due to the loss of slow atoms in a supersonic beam if a selection technique is used, or a practical atom usage rate in any case. The detection system inherently introduces a loss of photons, and the background noise degrades the signal to noise ratio. These limitations lead us to a limit in the loss of density that can be tolerated in the scheme to achieve a slow atom distribution.

Ultimately, the objective of the scheme is not to get the best densities with the slowest atoms, but to get adequate densities with slow enough atoms. For future experiments, perhaps a one atom laser, an atom trap may be in order, where a relatively large density can be achieved for a long time with narrow linewidths. This option, however, is probably

the costliest in time. We considered laser slowing, but in order to slow the entire distribution it would be necessary to slow beams an excessively long distance (close to two meters in most cases), which turns out to severely reduce density due to divergence of the atomic beam and transverse laser cooling. A novel scheme to use saturation spectroscopy may be possible, but densities would be limited to the velocity group densities already in the effusive beam, and the linewidths may be inherently broadened<sup>1</sup>. The same limitation of being confined to existing velocity group densities exists in velocity selection, but the densities needed may just be achievable based on the theory of Chapter 3. Since this is the easiest option to implement of those we considered, and preliminary estimates indicated that it should allow us to see the splitting, we decided to proceed with velocity selection.

## 1.5 Thesis Organization

This thesis is organized into five chapters. The first four chapters present background and the theoretical framework which guided the experiment. Chapter 5 includes the experimental data and analysis.

Chapter 1 should convey the context of the experimental work for this thesis. It explains why the thesis work was done.

The second chapter outlines a theory for coupled atom-cavity oscillator normal mode splitting. It is not intended to be detailed or rigorous since it is somewhat outside the scope of the thesis except for the fact that it provides the motivation for the work.

The theory needed to build the velocity selector to parameters which would provide an adequate atomic velocity profile is the subject of Chapter 3. Key to the design of the velocity selector is the loss of atomic density which is studied in detail.

Chapter 4 applies the cavity Doppler effect to the theory presented in Chapter 2 to determine the velocity selector parameters needed to see the normal mode splitting.

---

<sup>1</sup>This idea was presented by Daniel Heinzen while he was visiting MIT

Finally, Chapter 5 presents experiments we ran to see how well the velocity selector would work in practice and determine if the density would be adequate for our atom-cavity work.

## Chapter 2

# Basic Theory of Normal Mode Splitting

The scope of this thesis does not include a detailed development of atom-cavity theory, but a physical understanding of the conditions for normal mode splitting is certainly necessary, and an appreciation of the semiclassical theory which has guided our efforts puts the thesis work in proper context. With this in mind, an oversimplified coupled oscillator model is adequate then to derive what turns out to be the correct quantum mechanical expression for the coupling rate. This model is used to describe the atom-cavity experiments designed to measure the splitting. After that, the initial equations and spectral response of the more complete semiclassical model are presented, and the splitting condition is derived.

### 2.1 Simple Coupled Oscillator Model

The atom-cavity system will be modeled as an atomic oscillator which emits radiation at precisely frequency  $\omega$ , and a closed cavity field oscillator which sustains a mode only at this same frequency  $\omega$ . This corresponds to a cavity of infinite  $Q$  coupled to an atom of infinitesimal linewidth. This system turns out to meet the criteria for splitting

automatically, since decay, or damping, has been neglected. It cannot be used to derive the requirements for normal mode splitting, but it does give a simple physical picture. The coupled oscillator equations are:

$$\ddot{E} + \omega^2 E = \left( \frac{4\pi\omega^2}{V} \right) p \quad (2.1)$$

$$\ddot{p} + \omega^2 p = \left( \frac{e^2}{m} \right) E \quad (2.2)$$

where  $E$  is the electric field,  $V$  is the volume of the cavity,  $p$  is the dipole strength of the atomic oscillator,  $e$  is the electron charge, and  $m$  is the electron mass. First, these equations should be made plausible.

The classical atomic oscillator equation (Equation 2.2) is widely known to be useful in deriving the general properties of spontaneous emission. The electron is assumed to be oscillating harmonically with a restoring force  $eE$ . This model is the classical analog the two-level ensemble averaged density matrix equations when damping is included. It differs in that it does not include the oscillator strength, which will be inserted later in the model, and it assumes an inversion of  $-1$ . While the ensemble averaged inversion equation is generally needed to correctly describe the two level system, the inversion is very nearly our assumed value of  $-1$  for the weakly excited atoms in our experiments.

The vacuum field oscillator equation (Equation 2.1) starts with Maxwell's Equations, as it must in a semiclassical treatment. Starting with Ampère's Law as modified by Maxwell (Equation 2.3) and Faraday's Law (Equation 2.4)

$$\nabla \times \mathbf{H} = \frac{4\pi}{c} \mathbf{J} + \frac{1}{c} \frac{\partial \mathbf{D}}{\partial t} \quad (2.3)$$

$$\nabla \times \mathbf{E} = -\frac{1}{c} \frac{\partial \mathbf{B}}{\partial t} \quad (2.4)$$

we consider a charge free region ( $\nabla \cdot \mathbf{D} = 0$ ) which has no magnetic susceptibility ( $\mathbf{H} = \mathbf{B}$ ), assume  $\nabla \times \mathbf{P} = 0$  and  $\mathbf{J} = \sigma \mathbf{E}$ , and using  $\mathbf{D} = \mathbf{E} + 4\pi \mathbf{P}$ , derive the wave

equation

$$\nabla^2 \mathbf{E} - \frac{4\pi\sigma}{c^2} \frac{\partial \mathbf{E}}{\partial t} - \frac{1}{c^2} \frac{\partial^2 \mathbf{E}}{\partial t^2} = \frac{4\pi}{c^2} \frac{\partial^2 \mathbf{P}}{\partial t^2} \quad (2.5)$$

Having assumed a lossless cavity, we actually have  $\mathbf{J} = 0$ , but we will retain  $\sigma$  for comparison with Equation 2.14 which includes loss. The optical resonator imposes boundary conditions which give a sinusoidal spatial dependence to the electric field, which propagates along the cavity axis in the paraxial approximation.

$$\mathbf{E} = E(t) \sin kz \hat{\mathbf{x}} \quad (2.6)$$

The single dipole gives the cavity a polarization density  $\mathbf{P} = p/V \hat{\mathbf{x}}$  which is very dilute. The rapidly varying oscillations of the harmonically oscillating dipole will be at the resonance frequency  $\omega$ , so we can write the polarization density with a slowly varying envelope  $\tilde{p}$ , giving  $\mathbf{P} = [\tilde{p}(t) \sin \omega t \sin kz]/V \hat{\mathbf{x}}$ . If we neglect all derivatives of  $\tilde{p}$  because it is both slowly varying and dilute [8][p. 100], the second time derivative of the polarization density reduces to

$$\frac{\partial^2 \mathbf{P}}{\partial t^2} = \left( -\omega^2 \tilde{p} \sin \omega t + 2\omega \frac{d\tilde{p}}{dt} \cos \omega t + \frac{d^2 \tilde{p}}{dt^2} \sin \omega t \right) \frac{\sin kz}{V} \hat{\mathbf{x}} \approx \frac{-\omega^2 p}{V} \hat{\mathbf{x}} \quad (2.7)$$

Substituting Equations 2.6 and 2.7 in the wave equation (Equation 2.5), we can integrate out the spatial dependence, which we are not interested in, and reduce the equation to the desired form

$$\ddot{E} + 4\pi\sigma \dot{E} + k^2 c^2 E = \left( \frac{4\pi\omega^2}{V} \right) p \quad (2.8)$$

The factor  $4\pi\sigma$  corresponds to the cavity linewidth, which we have assumed to be zero (the mirrors are perfectly reflecting, or have no "conductivity"). The factor  $k^2 c^2 = \omega^2$  is the cavity supported mode frequency. We have now arrived at the field oscillator equation (Equation 2.1). Although we have claimed that this is the vacuum field oscillator, we have in no way introduced the vacuum fluctuations or any driving field for that matter. But since we are now only solving for the normal modes, this is not a problem; one does

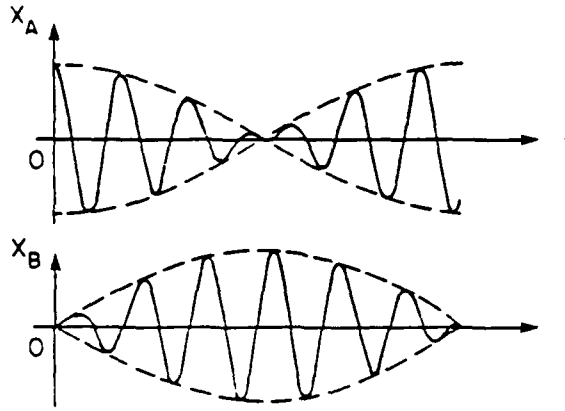


Figure 2-1: The Beat Frequency Associated With Two Weakly Coupled Oscillators. In the time domain, the amplitude of one of the oscillators slowly decreases relative to the oscillator frequency while the amplitude of the other oscillator increases. Hence energy is exchanged at a rate equal to half of the normal mode frequency difference.

not need to know the driver of a coupled oscillator system to derive the normal modes.

Since the system is two coupled oscillators, it is useful to imagine two coupled pendula as an analog. Since this system resonates at the normal mode frequencies and the pendula exchange energy at a rate equal to half the difference in frequency of the normal modes (see Figure 2.1), it is useful to solve for these normal modes. We do this by assuming a simultaneous solution to Equations 2.1 and 2.2 in which both pendula oscillate harmonically with the same phase and at the same frequency  $\Omega$ . Solving for  $\Omega$  we get

$$\Omega^2 = \omega^2 \pm \sqrt{\frac{4\pi\omega^2 e^2}{mV}} \quad (2.9)$$

If we now take the shift to be small, we find that to first order the oscillators exchange energy at the plasma frequency

$$\Omega = \omega \pm g \quad (2.10)$$

$$2g = \sqrt{\frac{4\pi e^2}{mV}} \quad (2.11)$$

Introducing the oscillator strength in the usual way [9][p. 218]

$$\frac{e^2}{m} \rightarrow f \frac{e^2}{m} = \frac{2\omega\mu^2}{\hbar} \quad (2.12)$$

we obtain an expression for  $g$  which is the same as one obtains for more rigorous quantum or semi-classical treatments

$$g = \frac{\mu}{\hbar} \sqrt{\frac{2\pi\hbar\omega}{V}} \quad (2.13)$$

The atom-cavity coupling rate has emerged quite naturally from the coupled oscillator equations. Since this quantity is to be measured when the cavity is tuned to the free space atomic resonance, it is not important that we assumed the cavity to support only that resonance. The other cavity modes are sufficiently removed in frequency space to have no effect. The closed cavity allowed us to write the polarization density as  $p/V$ ; in an open resonator an effective mode volume is computed which takes into account the different boundary conditions imposed by the open cavity. If the atom and cavity do not share the same resonant frequency, the expression for the frequency splitting becomes more complex, but it still depends on the  $g$  calculated above along with other terms.

## 2.2 Experimental Realization of Atom-Cavity Coupled Oscillators

The understanding of atom-cavity coupling as a coupled oscillator phenomenon is the basis for the larger atom-cavity experiment of our research group. Experiments exploring the atom-cavity coupling could explore either the time or frequency domain since coupled oscillators display measurable characteristic responses in either case. In the time domain, we would expect to see beating (Figure 2.1) at a rate determined by  $g$ , whereas in the steady state we expect to see resonances at the two normal modes split by a frequency that is a measure of  $g$ . Our current experiments, which are described briefly below, are in the steady state.

The basic components of the atom-cavity experiment are an atomic beam which supplies less than one atom on average into the cavity mode, a cavity defined by concentric spherical mirrors separated by 5 cm and with a reflectivity at the transition frequency of around 99%, a laser beam (Coherent 699 ring dye laser) which is at right angles to both the mirrors and atomic beam and which excites atoms near the center of the cavity, a reference beam from the same laser which excites atoms outside the cavity for comparison, collection optics, and a photon counting system (see Figure 1-1). As we scan the laser through the resonances of the system, we count photons emitted. The transition studied is the 553 nm  $^1S_0$  to  $^1P_1$  transition of barium. Our atom source is barium gas which escapes from a hole or slit in a heated steel or tantalum tube and is collimated into a beam by the use of apertures. The velocity distribution and density of this beam is very important in eliminating the cavity Doppler broadening and will be discussed in detail in Chapter 3. One of the cavity mirrors can be adjusted by three stacks of PZT's, and is locked to an iodine line with a second (Coherent 599) laser. The details of this setup will change for future experiments, but experiments will be similar in principle.

The laser beam which excites the barium atoms at the center of the cavity is the driving force of the coupled oscillator system; however, it does not saturate the atoms. It supplies energy to the system at the rate of spontaneous emission, a condition required by energy balance in the steady state. Thus the experiment is really an absorption experiment, although we measure fluorescence which occurs at an equal rate.

We have interpreted spontaneous emission as arising from the vacuum fluctuations of the cavity mode. If this interpretation were wrong and the mirrors did not influence the density of modes at the position of the atom, we would not see an alteration of the spontaneous emission rate nor would we see a two-peaked spectrum with the cavity tuned to the atomic center frequency. We could only expect to see the standard Lorentzian resonance lineshape of the uncoupled atomic oscillator. For an atom in a cavity not tuned to the atomic center frequency, we would expect to see a Rayleigh scattering peak, but we would not expect to see frequency pulling or atomic linewidth changes if the

system were not coupled. Since these changes for a non-resonant system are small, it is more convincing to actually achieve and measure the frequency splitting.

## 2.3 More Complete Semiclassical Theory and Splitting Conditions

The simple coupled oscillator model of Equations 2.1 and 2.2 lacks some critical features of the single atom - optical cavity system that did not affect the normal mode calculation. A more complete theory is included in the paper *Semiclassical Analysis of Single Atom Emission in an Optical Resonator*, authored by J.J. Childs, D.J. Heinzen, J.T. Hutton and M.S. Feld (to be published). Part of the theory included therein will be sketched here. First, to prevent any confusion about what is meant by strong atom-cavity coupling, we note that the coupling rate *is* always much less than an optical frequency, so the oscillators *are* always weakly coupled in the usual sense and *will* have normal modes split by twice the coupling rate. We will speak of strong or weak coupling in another sense, however. If the linewidths of the atom and cavity are not neglected, we find that splitting will not occur if the square of the difference of the linewidths is more than twice the square of the coupling rate. Furthermore, the splitting will not be resolvable if the linewidths are large compared to the splitting. Therefore we speak of the strong coupling limit when the coupling strength is large compared to the atom and cavity linewidths. As previously mentioned, a model that neglects linewidths, as did the one in Section 2.1, cannot predict the requirements for splitting, so the linewidths must be included.

Additionally, spontaneous emission was not present in the previous model, yet it is the energy source for the atom-cavity system. It is included by adding

a fluctuating dipole moment source  $G(t)$  having a Fourier transform  $g(\Omega) =$  (constant) with random varying phases ... to account for the vacuum fluctuations which initiate excited state decay. The constant multiplying  $G(t)$ , and the constant  $|g(\Omega)|^2 = \gamma_p/\pi$  are chosen such that the value of  $P(t)$  and its

Fourier transform  $p(\Omega)$  give the correct free space spontaneous emission rate for  $E = 0$ . [10]

With these elements included, the coupled oscillator equations 2.1 and 2.2 are generalized to take the following form:

$$\ddot{E} + 2\gamma_c \dot{E} + \omega_c^2 E = \left( \frac{4\pi\omega_c^2}{V} \right) p \quad (2.14)$$

$$\ddot{p} + 2\gamma_p \dot{p} + \omega^2 p = \left( \frac{2\mu^2\omega}{\hbar} \right) E + 4\omega\mu\sqrt{N_u}G \quad (2.15)$$

where  $N_u$  is the occupation probability of the excited state. By Fourier transforming the equations and assuming  $\Omega \approx \omega_c \approx \omega$ , the equations can be solved for the electric field in reciprocal space  $\mathcal{E}(\Omega)$ . The power output of the system as a function of a monochromatic driving laser frequency  $\Omega$

$$P_\omega(\Omega) = 2V\gamma_c \frac{|\mathcal{E}(\Omega)|^2}{8\pi} \quad (2.16)$$

can be written as the product of two Lorentzians

$$P_\omega(\Omega) = N_u \hbar\omega \left( \frac{\sigma_0 c}{V} \right) \left( \frac{\pi\gamma_c\gamma_p^2}{\Gamma_+\Gamma_-} \right) \mathcal{L}_+ \mathcal{L}_- \quad (2.17)$$

with  $\mathcal{L}_j$  a normalized Lorentzian lineshape of width  $\Gamma_j$  centered at  $\Omega = \Omega_j$

$$\mathcal{L}_j = \frac{\left( \frac{\Gamma_j}{\pi} \right)}{\left[ (\Omega - \Omega_j)^2 + \Gamma_j^2 \right]} \quad (2.18)$$

and  $\sigma_0$  the on-resonance value of the stimulated emission cross section. The peaks of the two Lorentzians are split by a frequency  $2I$ , where

$$2I = -\Theta^2 + \sqrt{\Theta^4 + 4\omega_-^2 \gamma_-^2} \quad (2.19)$$

$$\Theta^2 = -g^2 - (\omega_-^2 - \gamma_-^2) \quad (2.20)$$

with  $\omega_-$  and  $\gamma_-$  defined by  $\omega_- = (\omega_c - \omega)/2$  and  $\gamma_- = (\gamma_c - \gamma_p)/2$ . If we are to observe splitting for zero atom-cavity detuning ( $\omega_- = 0$ ),  $I$  must be nonzero (by definition), which means we must have  $\Theta^2 < 0$ . This establishes a splitting condition for an atom-cavity system at zero detuning:

$$g^2 > \left( \frac{\gamma_c - \gamma_p}{2} \right)^2 \quad (2.21)$$

When this condition is met, the linewidths of the two Lorentzians,  $\Gamma_+$  and  $\Gamma_-$ , are both equal to the average of the atom and cavity linewidth. While the above condition guarantees that the two Lorentzians are peaked at different frequencies, it does not guarantee that their product will exhibit local maxima at those peaks. This can be done by showing that the derivative of  $P_\omega(\Omega)$  vanishes at  $\Omega = \Omega_+, \Omega_-$ , and  $\omega$ , and requiring the second derivative of  $P_\omega(\Omega = \omega)$  to be negative. This establishes a second splitting condition

$$g^2 > \frac{\gamma_c^2 + \gamma_p^2}{2} \quad (2.22)$$

The two splitting conditions can be summarized for most practical purposes by the single condition

$$g > \gamma_c, \gamma_p \quad (2.23)$$

## 2.4 The Splitting Condition in Terms Of Cavity Parameters

The splitting requirement for a degenerate cavity reduces to a product of cavity finesse and the solid angle. The splitting condition can be rewritten in terms of atom-cavity system parameters to make this assertion more transparent. We will use the on resonance value of the stimulated emission cross section

$$\sigma_0 = \frac{8\pi\omega\mu^2}{\hbar c(2\gamma_p)} \quad (2.24)$$

the free spectral range expressed in Hertz

$$\Delta_{\text{FSR}} = \frac{c}{2l} \quad (2.25)$$

and a solid angle factor

$$f = \frac{3}{4}\theta_{\text{beam}}^2 \quad (2.26)$$

The effective mode volume is determined by a diffraction limited waist as discussed in Chapter 1

$$V = \pi \rho_0^2 l = \pi \left( \frac{\lambda}{\pi \theta_{\text{beam}}} \right)^2 l = \frac{3\lambda^2 l}{4\pi f} \quad (2.27)$$

Substituting this expression for the effective mode volume, we arrive at a new expression for  $g$ .

$$g = \frac{\mu}{\hbar} \sqrt{\frac{2\pi \hbar \omega}{V}} = \sqrt{\left( \frac{8\pi \omega \mu^2}{\hbar c (2\gamma_p)} \right) \left( \frac{2\pi}{3\lambda^2} \right) \left( \frac{c}{2l} \right) (2\gamma_p f)} \quad (2.28)$$

Since the atom is damped by only radiative processes to a good approximation, the first two terms in parenthesis cancel since they are both expressions for the on resonance stimulated emission cross section, allowing us to write

$$g = \sqrt{2\Delta_{\text{FSR}}\gamma_p f} \quad (2.29)$$

If we consider the case in which the atomic and cavity linewidths to be equal, and introduce the cavity finesse  $\mathcal{F} = \pi\Delta_{\text{FSR}}/\gamma_c$ , we can express the splitting condition  $g > \gamma_c, \gamma_p$  in a very simple way:

$$\mathcal{F}f > \frac{\pi}{2} \quad (2.30)$$

In this form it is easy to see why we cannot arbitrarily cut down our solid angle to reduce the Doppler broadening. It is a consequence of our decision to achieve strong coupling by using a degenerate resonator. In our experiments,  $\gamma_c$  is always somewhat greater than  $\gamma_p$ , which requires us to achieve a slightly higher value of  $\mathcal{F}f$  than  $\pi/2$ .

## Chapter 3

# Velocity Selector Theory

### 3.1 General Theory of Operation<sup>1</sup>

Our velocity selector consists of a rotating cylinder with several helical slots around its radius (see Figure 3-1). Atoms that enter a slot must have an appropriate speed to pass through the slot without hitting the sides and being eliminated from the beam. Multiple wheels are also sometimes used, but such a velocity selector must be carefully designed to ensure that atoms of an unselected speed cannot travel through a “wrong” sequence of slots and pass through the apparatus. Since a solid cylinder velocity selector can have channels spaced arbitrarily close without allowing these harmonics, it is probably a better design for achieving a higher flux.

Notation used to explain the theory of the velocity selector is illustrated in Figure 3-1. It is assumed that all of the atoms in the beam are travelling parallel to the axis of the velocity selector. Since the atomic density at the velocity selector is much less than that in the oven, collisions between atoms are assumed to be negligible. An atom of velocity  $v_0$  that passes through the velocity selector without changing its position relative to the

---

<sup>1</sup>The theory of Section 3.1 is taken primarily from Reference [11]

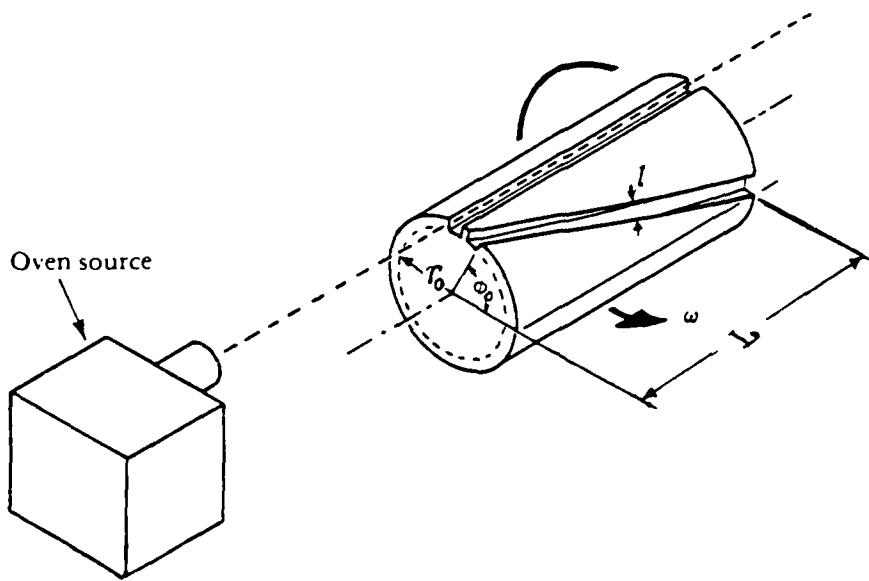


Figure 3-1: Velocity Selector. Only one helical channel is shown for clarity

walls of the slot will satisfy the equation

$$v_0 = \frac{\omega L}{\phi_0} \quad (3.1)$$

The quantity  $L/\phi_0$  is characteristic of the pitch at which the slots were cut. The angular velocity of the velocity selector,  $\omega$ , can be chosen to select a particular  $v_0$  which we will call the selected velocity.

Since the slots have a finite width  $l$ , atoms in a range  $v_{min} = \omega L/\phi_{max}$  to  $v_{max} = \omega L/\phi_{min}$  will be transmitted, provided they enter the slot at an appropriate point. In the reference frame of the atom, atoms within this range are traveling at varying angles through a straight channel. The fastest atoms transmitted enter at one edge of the channel and exit at the opposite edge, while the velocity selector has turned an angle

$$\phi_{min} = \phi_0 - \left( \frac{l}{r_0} \right) \quad (3.2)$$

with  $r_0$  the mean radius of the velocity selector slots. By adding rather than subtracting from  $\phi_0$  one obtains an expression for  $\phi_{max}$ . The maximum and minimum transmitted

velocities can now be expressed as fractions of the selected velocity  $v_0$

$$v_{min} = \frac{v_0}{1 + \gamma} \quad (3.3)$$

$$v_{max} = \frac{v_0}{1 - \gamma} \quad (3.4)$$

$$\gamma = \frac{l}{\phi_0 r_0} \quad (3.5)$$

The quantity  $\gamma$  is a fixed property of the velocity selector.

Atoms traveling at exactly the maximum or minimum velocities must enter the velocity selector at exactly the appropriate edge to pass through. We can say that they have an effective aperture that goes to zero. This suggests that we define a reduction factor  $A(v)$  which is the ratio of an effective slot aperture  $l'$  for an atom traveling at velocity  $v$  to the actual aperture width  $l$ . The difference of the effective and real slot apertures

$$l - l' = r_0 |(\phi_0 - \phi(v))| \quad (3.6)$$

leads us to the reduction factor

$$A(v) = \frac{l'}{l} = \begin{cases} 1 - \frac{1}{\gamma} \left| 1 - \frac{v_0}{v} \right| & \text{if } v_{min} < v < v_{max} \\ 0 & \text{otherwise} \end{cases} \quad (3.7)$$

If we define the resolution of the velocity selector to be  $\Delta v/v_0$  at  $A(v) = \frac{1}{2}$ , we can show from Equation 3.7 that the resolution has the value of the velocity selector parameter  $\gamma$  defined in Equation 3.5. In the remainder of the text, I will use the terms  $\gamma$  and resolution interchangeably.

## 3.2 Density Reduction

The velocity selector eliminates virtually all atoms outside of the selected velocity interval and a large portion of those in the interval. If one is selecting a velocity interval in which

there are relatively few atoms to begin with, it is apparent that the density loss could be severe. This section examines the theoretical density reduction due to the distance the oven is from the interaction region, perhaps increased by the introduction of a velocity selector, and from the operation of the velocity selector itself.

### 3.2.1 Beam Divergence

In the effusive beam limit, atoms emerge from the oven unaffected by the aperture. In this limit, the aperture dimensions are less than a mean free path, so we get very few collisions at the aperture and atoms continue to travel in the same direction they were previously headed. If we assume the oven aperture to have a negligible affect on thermal equilibrium, the velocity distribution will be Maxwell-Boltzmann, but this distinction is unimportant in this section. As the beam becomes supersonic, it becomes more directional and the velocity distribution tends to narrow because of collisions in the vicinity of the oven aperture [12][328-329]. Since we desire to achieve a slow atom distribution, we focus on the effusive beam.

For a given oven aperture, the atomic beam will increase in overall density as the temperature is raised, but the density of slow atoms will decrease once the beam becomes supersonic. The atoms inside the oven can be assumed to compose an ideal gas in thermal equilibrium with the solid. Using the ideal gas law, the oven density is  $n_o = P/(kT)$ , where  $P$  is the vapor pressure, which increases with temperature exponentially.

Using an averaged velocity,  $\bar{v}$ , for simplicity, the number of atoms per second emerging from an oven with an aperture of area  $A_o$  into a solid angle  $\Omega$  is [13][p. 11]

$$\dot{Q} = \int \frac{d\Omega}{4\pi} n_o \bar{v} A_o \cos \theta \quad (3.8)$$

The  $\cos \theta$  term comes from the projection of the aperture and reduces the density off axis. If  $\dot{Q}$  atoms per second pass through the oven aperture, the same number of atoms will pass through an aperture some distance from the oven into the same solid angle. This aperture is the one that collimates the atomic beam and is assumed small enough

and at a great enough distance so that the density is essentially constant throughout the beam. The density reduction at this collimating aperture of area  $A'$  at a distance  $L$  from the oven is

$$\frac{n}{n_o} = \frac{\dot{Q}}{n_o \bar{v} A'} = \frac{1}{n_o \bar{v} A'} \frac{n_o \bar{v} A_o}{4\pi} \left[ \int_0^{2\pi} d\phi \int_0^{\theta'} d\theta \sin \theta \cos \theta \right] \quad (3.9)$$

For small angles, the integral tends to  $A'/L^2$  and the density reduction is independent of the collimating aperture dimensions.

$$\frac{n}{n_o} = \frac{A_o}{4\pi L^2} \quad (3.10)$$

The density is seen to increase linearly with the oven aperture area and decrease in proportion to the square of the distance between the source and region of interest. Naively applying these results one would minimize the distance from the oven and use a large aperture. To get the maximum density of atoms in the beam, however, we want to heat the atoms to the highest temperature consistent with an effusive beam, since vapor pressure increases with temperature. But if we selected a smaller aperture, we could heat the atoms to a higher temperature and still have an effusive beam. Because of this tradeoff, the aperture size and geometry should be optimized to achieve the maximum beam density in the effusive limit.

### 3.2.2 Velocity Selection Density Reduction

As successive slots on the velocity selector sweep through the atomic beam, pulses of atoms are created. This does not last long, however, as the beam tends to become uniformly dense as the atoms in each pulse spread out due to their different velocities and overlap other pulses. The density for atoms at a given velocity is reduced by the ratio of the slot width to the distance between the slots, and also by the effective aperture reduction factor  $A(v)$ .

Fluorescence is proportional to the density of atoms in the beam since the interaction volume is defined by an aperture and a laser beam. It is therefore the density of atoms

for given velocity selection parameters that we are interested in. Without the velocity selector, the density distribution is described by the normalized Maxwell-Boltzmann speed distribution given the assumptions of the effusive beam.

$$n_o(x) = n_o G(x) \quad (3.11)$$

$$G(x) = \frac{4}{\sqrt{\pi}} x^2 e^{-x^2} \quad (3.12)$$

where  $x = v/u_{th}$  and  $u_{th} = \sqrt{2kT/M}$ . Assuming the holes and slots on the velocity selector to be evenly spaced, the velocity selected density will be reduced by the beam divergence factor and integrated effective aperture factor in addition to the trivial reduction of  $\frac{1}{2}$ . The effective aperture reduces the total density by the factor

$$\frac{n}{n_o} = \frac{1}{2} \frac{4}{\sqrt{\pi}} \int_{\frac{\alpha}{1+\gamma}}^{\frac{\alpha}{1-\gamma}} dx x^2 e^{-x^2} \left[ 1 - \frac{1}{\gamma} \left| 1 - \frac{\alpha}{x} \right| \right] \quad (3.13)$$

The factor  $\alpha$  is the selected velocity as a fraction of  $u_{th}$ :  $\alpha = v_o/u_{th}$ . The integral can be solved by expanding the exponential in a power series, giving

$$\frac{n}{n_o} = \frac{1}{2} \frac{4}{\sqrt{\pi}} \sum_{k=1}^{\infty} \frac{(-)^{k+1} \alpha^{2k+1}}{\gamma(k-1)!(2k)(2k+1)} \left[ \frac{1}{(1+\gamma)^{2k}} + \frac{1}{(1-\gamma)^{2k}} - 2 \right] \quad (3.14)$$

which in explicit form looks like

$$\frac{n}{n_o} = \frac{2}{\sqrt{\pi}} \left\{ \frac{\alpha^3}{6\gamma} \left[ \frac{1}{(1+\gamma)^2} + \frac{1}{(1-\gamma)^2} - 2 \right] - \frac{\alpha^5}{20\gamma} \left[ \frac{1}{(1+\gamma)^4} + \frac{1}{(1-\gamma)^4} - 2 \right] + \dots \right\} \quad (3.15)$$

In the limit of small  $\gamma$  and small  $\alpha$ , the expression reduces to

$$\frac{n}{n_o} = \frac{2}{\sqrt{\pi}} \gamma \alpha^3 \quad (3.16)$$

Unfortunately, this limit is not always applicable to this work.

## 3.3 Velocity Selector Design

### 3.3.1 Selection of Resolution

The primary shortcomings of the velocity selector when it is used to select out a slow distribution cannot be overcome by design. Because of the  $v^2$  dependence of the Maxwell speed distribution which dominates at low speeds, a loss is always incurred of order  $\alpha^3$ . Since  $\alpha$  is determined by the maximum acceptable average velocity to meet the splitting requirements, it cannot be sacrificed to reach acceptable densities. The resolution of the velocity selector,  $\gamma$ , affects the density linearly to lowest order in  $\gamma$ . When  $\gamma$  is relatively large, however, the higher order terms significantly increase the density over the lowest order factor of  $\gamma$ . It is not hard to see why this is so. For small  $\gamma$ , the range of the effective aperture function,  $A(x)$ , is small compared to the width of the Gaussian speed distribution. The value of the Gaussian varies little over the range of  $A(x)$ , so it can be pulled out of the integral and evaluated at the peak of  $A(x)$ , which is  $\alpha$ . The remaining integral evaluated to first order is just  $\gamma\alpha$ . When  $\gamma$  is not small, however, the range of  $A(x)$  is such that  $G(x)$  is *not* nearly constant, and the Gaussian is increasing more rapidly towards the center of the distribution than it is falling off on the wings.

The net result of this for a low resolution velocity selector is twofold: first, density is significantly greater than would be predicted by the first order result, and second, the average velocity of the reduced signal is shifted towards the most probable velocity of the Gaussian from the selected velocity  $\alpha$ . Since density is a critical consideration in the successful completion of our experiment, it is important to understand the effect of a low resolution velocity selector. For values of  $\alpha$  much over 25% the density reduction factor series, Equation 3.14, converges slowly, so a computer was needed to aid in computation. The relationship between the density reduction and the parameters  $\alpha$  and  $\gamma$  is shown in Table 3.1 in Figure 3-2.

The second affect of a broad resolution velocity selector is that the average velocity is shifted towards the center of the Gaussian speed distribution. As compared to a narrow

	$\gamma = .05$	$\gamma = .20$	$\gamma = .40$	$\gamma = .60$	$\gamma = .80$
$\alpha = .05$	$2.93 \times 10^{-7}$	$1.29 \times 10^{-6}$	$3.63 \times 10^{-6}$	$1.12 \times 10^{-5}$	$7.30 \times 10^{-5}$
$\alpha = .20$	$7.22 \times 10^{-5}$	$3.17 \times 10^{-4}$	$8.79 \times 10^{-4}$	$2.58 \times 10^{-3}$	$1.31 \times 10^{-2}$
$\alpha = .40$	$1.02 \times 10^{-3}$	$4.45 \times 10^{-3}$	$1.18 \times 10^{-2}$	$3.03 \times 10^{-2}$	$8.71 \times 10^{-2}$
$\alpha = .60$	$4.24 \times 10^{-3}$	$1.81 \times 10^{-2}$	$4.51 \times 10^{-2}$	$9.60 \times 10^{-2}$	$1.74 \times 10^{-1}$
$\alpha = .80$	$1.01 \times 10^{-2}$	$4.24 \times 10^{-2}$	$9.73 \times 10^{-2}$	$1.72 \times 10^{-1}$	$2.41 \times 10^{-1}$

Table 3.1: Density Reduction Factor for Various Values of  $\alpha$  and  $\gamma$

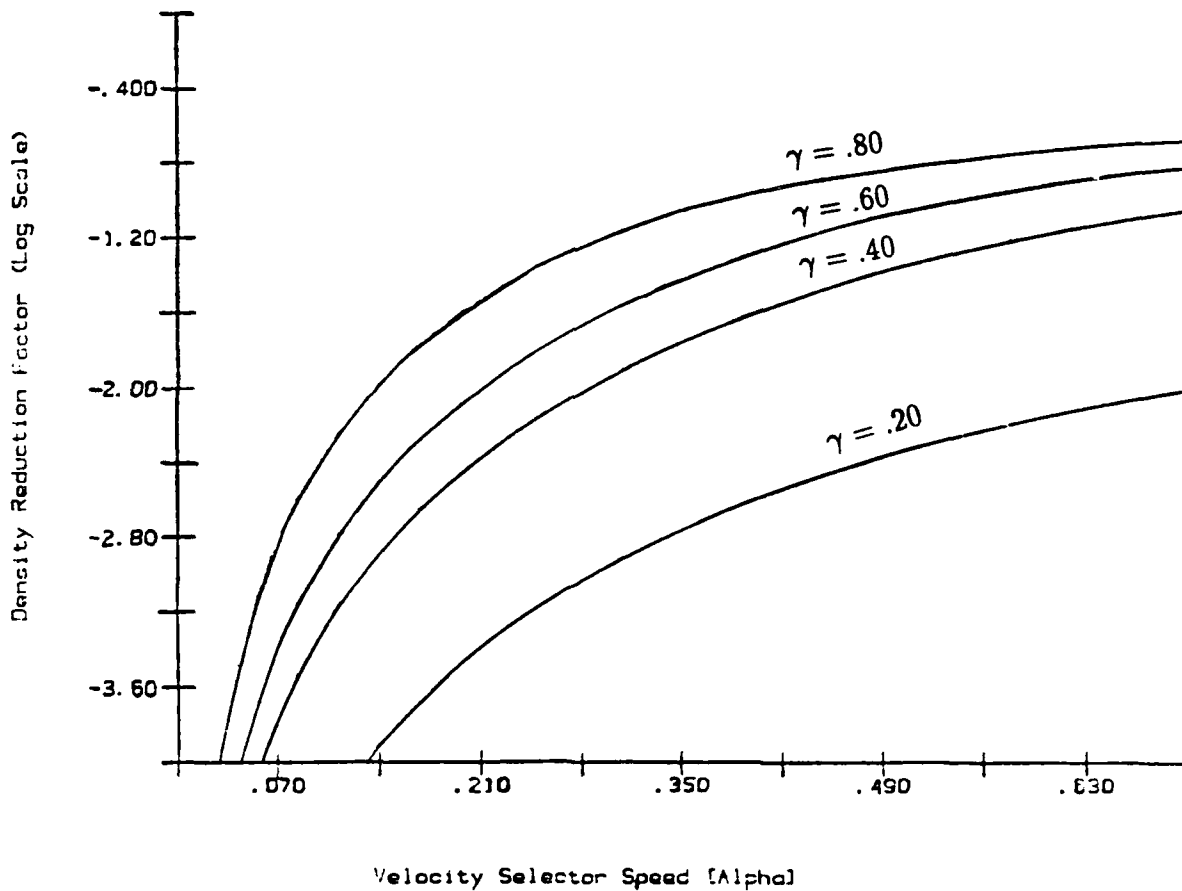


Figure 3-2: Density Reduction Versus  $\alpha$  for Various Values of  $\gamma$

	$\gamma = .05$	$=.20$	$=.40$	$=.60$	$=.80$
$\alpha = .05$	.050	.052	.058	.075	.13
$=.20$	.20	.21	.23	.29	.49
$=.40$	.40	.41	.46	.57	.78
$=.60$	.60	.62	.68	.80	.95
$=.80$	.80	.82	.88	.98	1.1

Table 3.2: Effective Dimensionless Velocity  $\bar{\alpha} = \bar{v}/u_{th}$  for Various Values of  $\alpha$  and  $\gamma$

resolution velocity selector,  $\alpha$  will be effectively higher. If we use a velocity selector with a high value of  $\gamma$ , we will have to select a lower speed than we would if we were using a velocity selector with a low value of  $\gamma$  to achieve the same average velocity. The dimensionless average velocity  $\bar{\alpha}$  expressed as a fraction of thermal velocity can be computed by dividing the atomic beam flux by its density.

$$\bar{\alpha} = \frac{\int dx xG(x)A(x)}{\int dx G(x)A(x)} \quad (3.17)$$

The denominator is evaluated in Equation 3.14, and the numerator can be expressed as a similar infinite sum

$$\Phi = n_0 \frac{1}{2} \frac{4}{\sqrt{\pi}} \sum_{k=1}^{\infty} \frac{(-)^{k+1} \alpha^{2k+2}}{\gamma(k-1)!(2k+1)(2k+2)} \left[ \frac{1}{(1+\gamma)^{2k+1}} + \frac{1}{(1-\gamma)^{2k+1}} - 2 \right] \quad (3.18)$$

Table 3.2 shows how this average dimensionless velocity  $\bar{\alpha}$  increases for fixed  $\alpha$  and increasing  $\gamma$ .

The effect of introducing a velocity selector into the atom-cavity experiment, as discussed in Chapter 4, is not as simple as merely incorporating an average velocity, but the above results should be useful as a guide nonetheless. For experiments conducted as part of this thesis, a velocity selector with a resolution of  $\gamma = .44$  was used, but several considerations not related to this theory resulted in our particular velocity selector design, and many of the calculations in Chapter 4 had not been made.

### 3.3.2 Construction of Velocity Selector

It had not been clear from the beginning that a velocity selector would give us adequate densities to resolve the splitting even if the splitting conditions were met. In addition to the theoretical problem of how the coupling strength is affected by the cavity Doppler effect, we thought we might have too much noise to extract a measurable signal. In order to determine if we would have enough density to get an adequate signal and to determine how well a velocity selector would work in the atom-cavity experiment, we decided to add a velocity selector to the experiment in the simplest way possible.

The vacuum cavity which encloses the oven and resonator has limited space to add a velocity selector. This limitation precluded us from using a velocity selector that we already had with a resolution of about  $\gamma = .075$  without some modifications. It would be necessary to either build an extension to the vacuum chamber, which would decrease density by a factor of  $1/L^2$ , or to modify the velocity selector. As can be seen in Figure 3-4, the space limitation is quite severe. The simplest modification was to collapse the five fins of the velocity selector which were spread out over a distance of 2 inches into a single cylinder  $\frac{1}{4}$  inch long. This had the further advantage of increasing the density we could expect by an order of magnitude because of the poorer resolution. Because of the slight increase in  $\bar{\alpha}$ , however, this gain was somewhat offset by the need to select slightly slower atoms (see Table 3.2). Computer plots presented at the end of Chapter 4 show that we should be able to resolve the splitting for  $\alpha = .15$  or  $\alpha = .2$  for this resolution velocity selector.

Because of the space limitations, our velocity selector is not directly coupled to the motor, but rather is belt driven. Some additional vibration has been added to the system, and we have had trouble with the belt coming off when it was not well aligned. The motor is inside the vacuum chamber where it is water cooled by copper tubes fed through the chamber wall. The motor temperature is monitored by a thermocouple, and has a steady state temperature of only about 20°C. Both the motor and the velocity selector are lubricated with Braycote 601 low vapor pressure grease. The motor is a standard four

pole ac hysteresis synchronous motor, which was selected because it runs very precisely at half of the input frequency regardless of torque until a threshold is reached.

Vibrations are not a problem for the experiments of this thesis, but they will certainly be a significant problem to overcome when the optical cavity is introduced into the chamber. Two principle problems exist with vibration isolation and damping. One is that most of the standard damping materials; rubber, felt, cork, foam, and rubberized synthetics to name a few, outgas at too great a rate to use in a vacuum. We tried Teflon, but it took a long time to pump down and became stiff after it had outgassed to a steady state level. The second problem is that the natural frequency of most damping materials is around 20 Hz, which is about the speed we run our velocity selector for an  $\alpha$  of about 5%. A velocity selector run at a higher speed, on the other hand, vibrates more. Although we have not found a material yet that seems really suitable for adequately damping the velocity selector inside the vacuum chamber, the best material we have found seems to be viton o-rings placed so that neither the vacuum chamber nor the bolts that go into the floor of the chamber are in direct contact with the velocity selector or motor mounts.

Alignment of the oven hole with the interaction region aperture and the directing of the laser beam onto the atomic beam would be difficult with the reduced density from a selected beam. Even more serious would be the problem of locking the laser feedback circuit to the reduced reference signal or even acquiring it through the optical fiber bundle. Usually a straight slot as drawn in Figure 3-1 is used to solve the first problem, but we still would not be able to lock the laser. We were also not sure we could control the rotation of the velocity selector precisely enough inside the vacuum chamber to align such a slot. So, instead, we have built a translation stage into the mount with a mechanical feedthrough through the top cover to raise and lower the velocity selector (see Figures 3-5, 3-6, and 3-8 at the end of the chapter). We only have to raise or lower the velocity selector a small distance, so the belt has not been a problem. The oven, velocity selector, and interaction region aperture are adjusted so that the velocity selector can block the beam to the region being studied, but does not block the reference beam signal

(see Figure 3-3). Once the velocity selector is started, a selected atom distribution goes through the interaction region aperture and an unselected distribution is excited at the reference signal. This system has worked quite well.

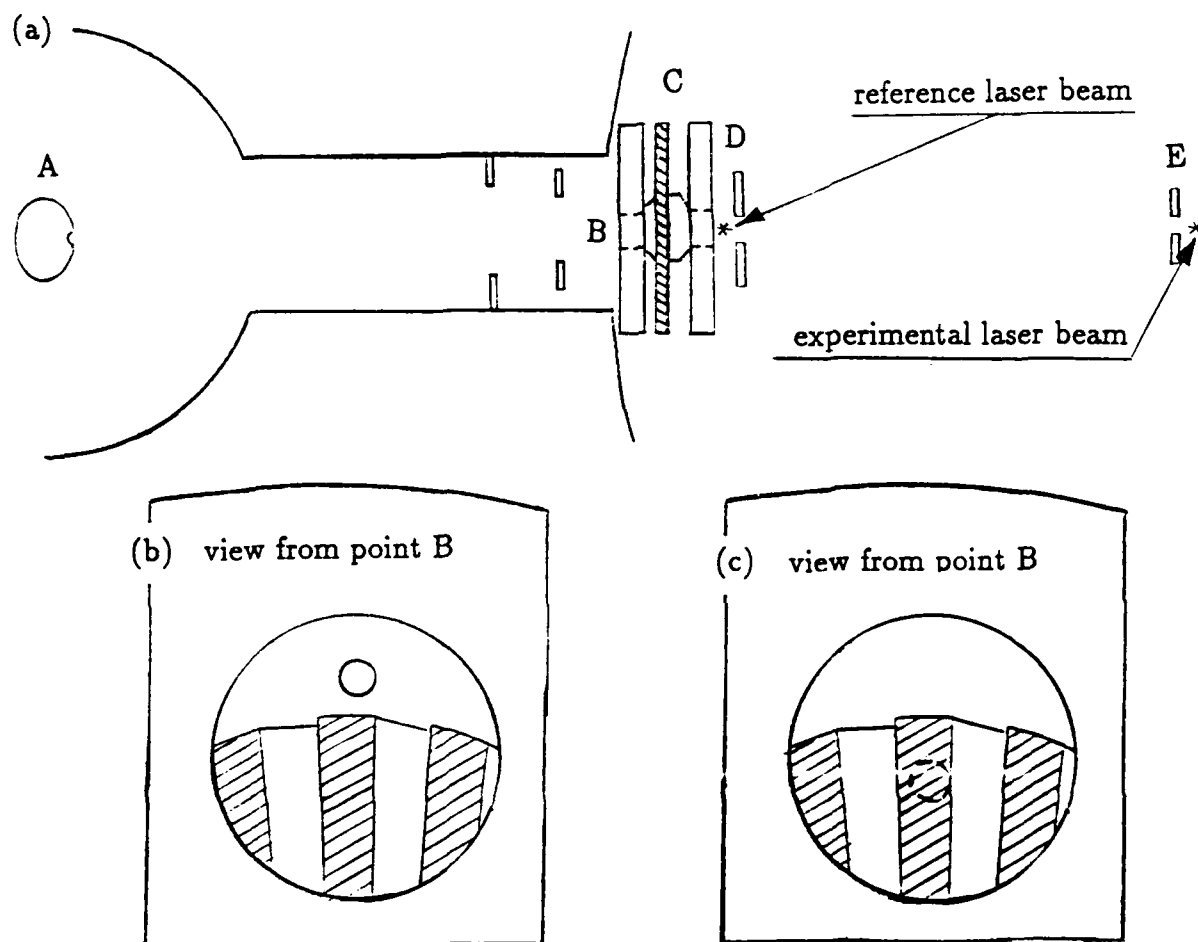


Figure 3-3: Velocity Selector "On-Off" Switch. (a) The path an atom takes from the oven (A), through the velocity selector (C), and through two  $800\mu\text{m}$  apertures (D and E). The reference laser beam is before the first aperture and the experimental laser beam is after the second one. (b) With the velocity selector lowered, an atom can pass through the  $800\mu\text{m}$  apertures (represented by the small circle) without passing through the velocity selector slots. (c) With the velocity selector up, the atomic beam must pass through the velocity selector to reach the experimental laser beam, but atoms passing above the velocity selector are still excited by the reference beam

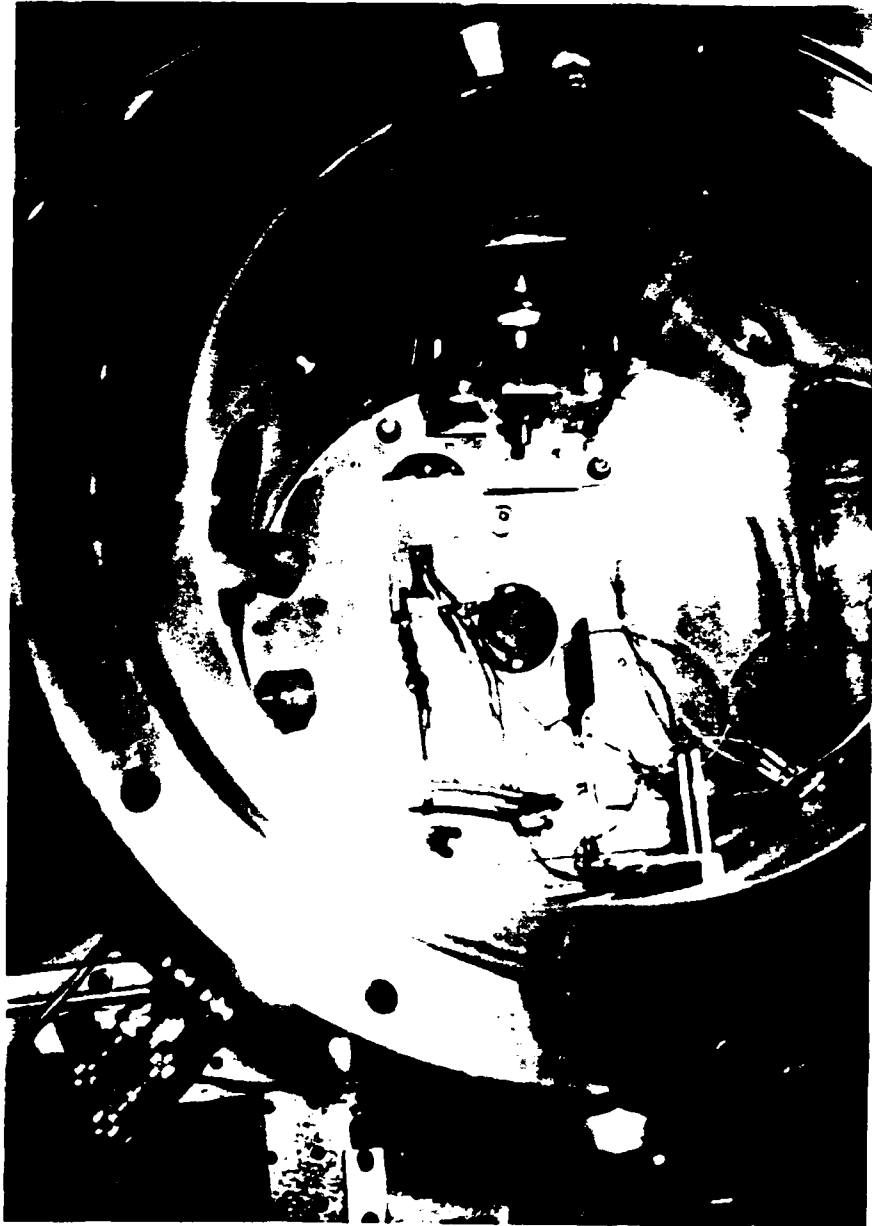


Figure 3-4: Velocity Selector and Motor inside the Vacuum Chamber. You can see the cooling lines to the motor and the close positioning of the velocity selector to the vacuum chamber walls. The resonator structure (not shown) straddles the motor and is within  $\frac{1}{8}$  inch of the velocity selector



Figure 3-5: Side View of the Velocity Selector Showing the Translation Stage and Feedthrough Rod



Figure 3-6: Back View of the Velocity Selector

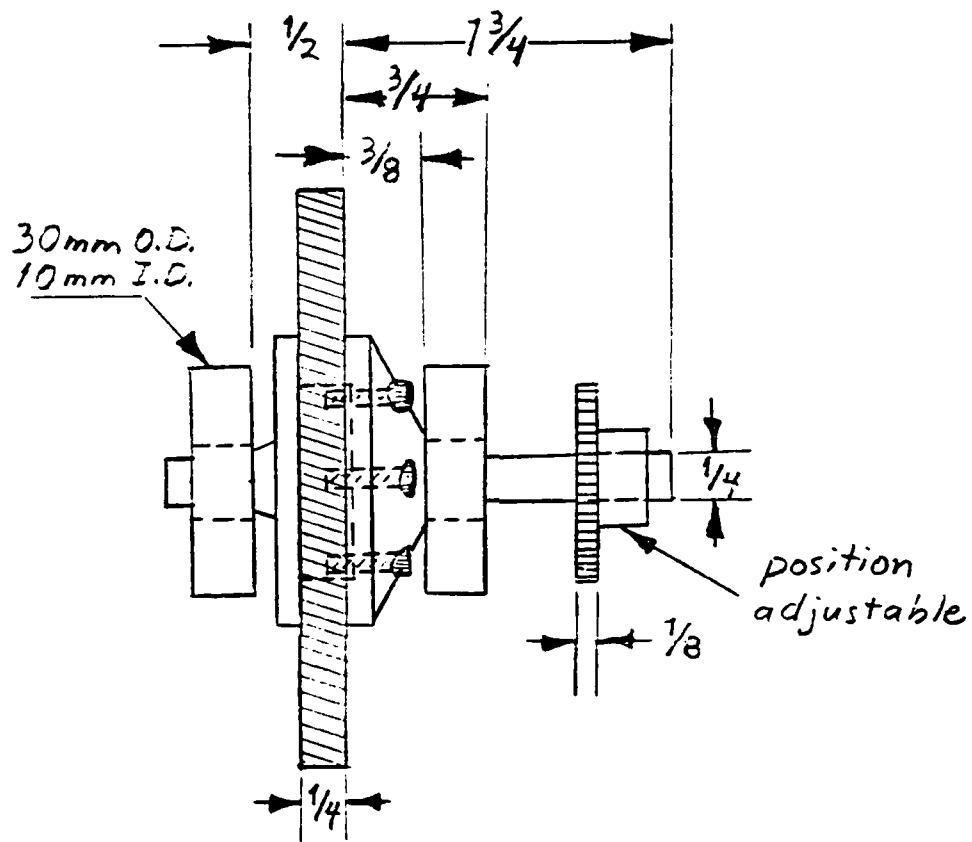


Figure 3-7: Velocity Selector Outside of the Mount. You see in profile the velocity selector channels, two ball bearings, and the pulley.

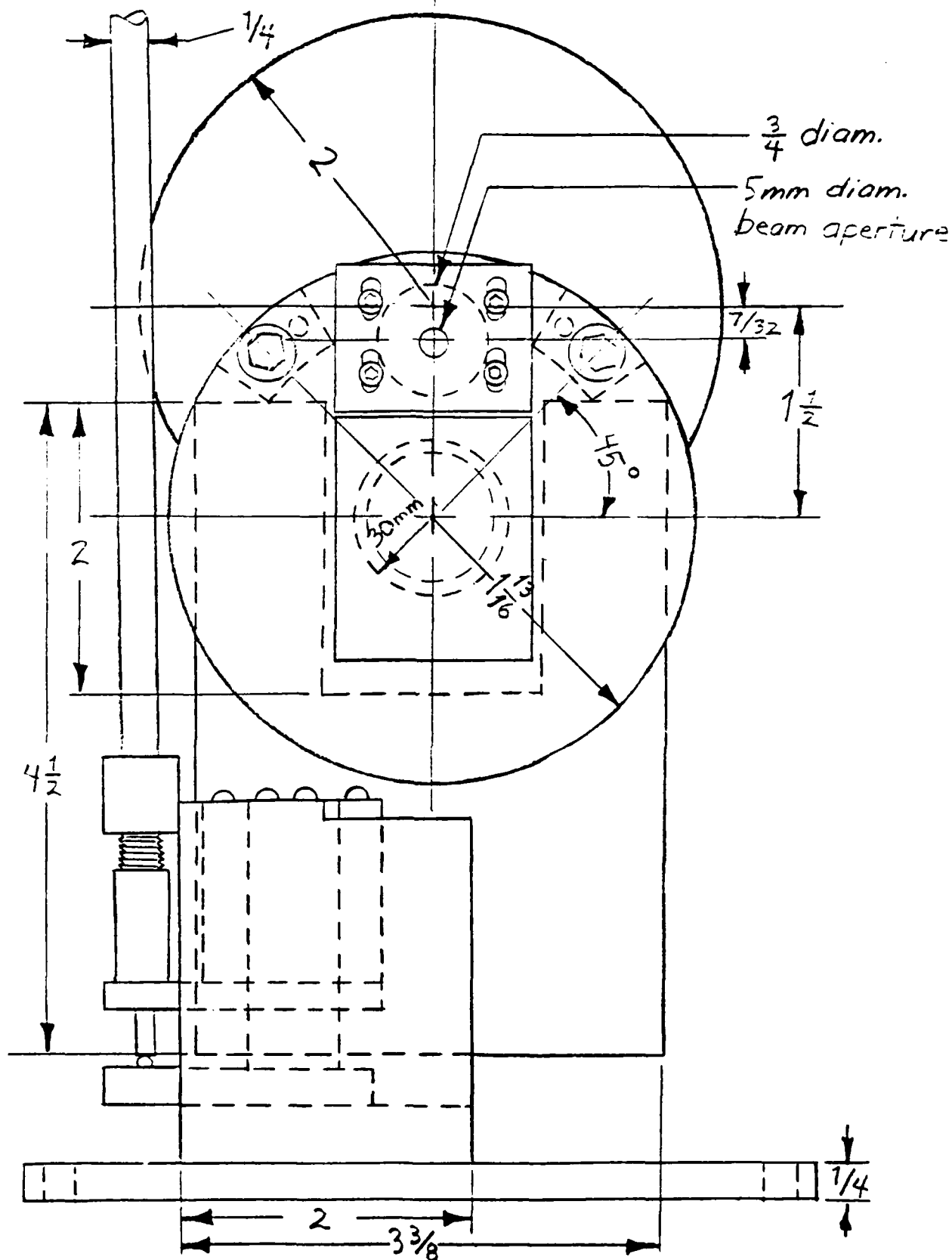


Figure 3-8: Velocity Selector Mount. The uppermost portion is a light baffle. The hole for the ball bearing is covered to keep barium out. You can see the translation stage on the left side.

## Chapter 4

# Cavity Doppler Effect Theory

### 4.1 The Cavity Doppler Effect

The relative motion of the atomic beam to the mirrors affects the coupled atom-cavity oscillator equations in two basic ways. The first is simply that the cavity is resonant with the moving atomic dipole at angle dependent Doppler shifted frequencies (see Figure 4-1). The atom and the cavity respond differently to this Doppler shift. If the atom emits a wave traveling toward a mirror it is approaching, it sees an image emitting radiation that is red shifted. From the reverse direction, from which the light is returning in phase after one transit, the atom sees the red shifted radiation blue shifted back into resonance with the atom, since the atom is moving away from that mirror. Thus the resonant behavior of the atom is the same as without considering motion. In contrast, the cavity sees a photon that is Doppler shifted depending on angle because there is relative motion of the cavity towards or away from the radiation source except in the plane perpendicular to the atomic beam. When a frequency is emitted by the atom that is Doppler shifted into resonance with a particular part of the mirror, the transmission probability will be maximum for that part of the mirror. Since this can occur over a relatively large range of frequencies corresponding to different angles to the mirror, we see a broadened cavity peak at large atom-cavity detuning. Our experiments cannot distinguish the angle at

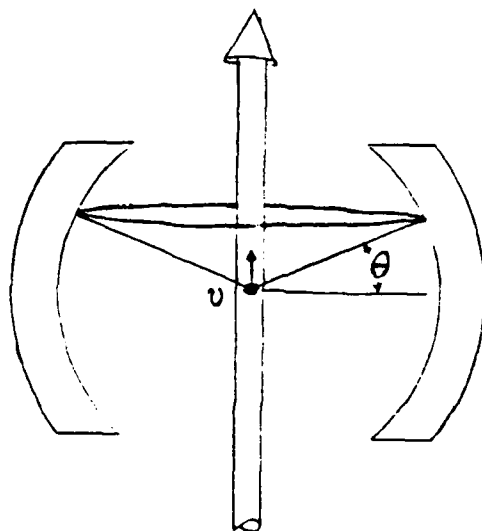
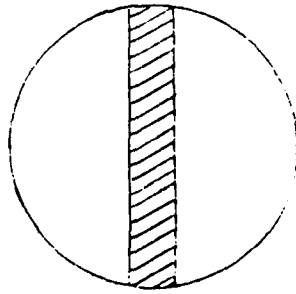


Figure 4-1: Cavity Doppler Effect. The parts of the mirrors which intersect the cone see the same Doppler shift for a given velocity atom. Only a two-dimensional slice of the spherical mirrors is shown

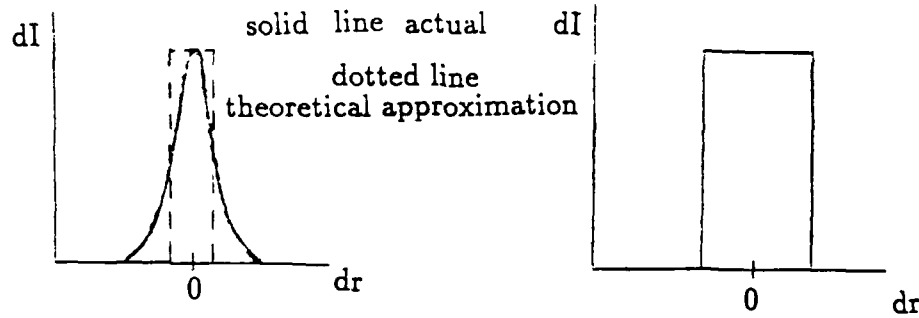
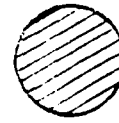
which the photon is emitted.

The second effect is more subtle. It decreases the atom-cavity coupling because the effective mode volume is increased. The coupling of the atom-cavity system is a resonant phenomenon, but a moving atom will not be coupled to the entire solid angle at a given frequency because outside of a certain angle  $\theta$  a photon will be Doppler shifted outside of the cavity resonance. Since diffraction determines the size of the waist at cavity center, this reduced solid angle translates to reduced coupling. This is really a simplified view, because there is no exact point at which something is resonant or non-resonant, but rather a continuum which is described by the Lorentzian lineshape. In estimating the coupling loss, however, we will assume that every part of the mirror within given limits is "resonant" and outside of those limits there is no coupling. The limits are defined by the half intensity point of the convolved atom and cavity Lorentzian. We have, in essence, substituted a constant function over certain limits for the resonant lineshape (see Figure 4-2). The coupling is equivalent to a stationary atom coupled to a smaller mirror. The mode volume, which is inversely proportional to the area of the mirrors, is

"Resonant" Area of the Mirror.



Equivalent Smaller Mirror Seen  
by a Stationary Atom



Intensity of light transmitted by the mirror  
as a function of linear position.

Figure 4-2: Resonant Area of a Cavity as Seen by a Moving Atom

increased by the the ratio of the full mirror area to the Doppler effect reduced mirror area. This ratio will be calculated in Section 4.3.

## 4.2 Modified Semiclassical Equations

The coupled atom-cavity oscillator equations (2.14 and 2.15) are easily modified based on the above discussion by adding a velocity and angular dependent Doppler shift of the cavity center frequency  $\omega_c$ . The mode volume  $V$  is also replaced by  $V'$  to represent that it is modified in accordance with the above discussion, but will not be explicitly calculated in this section. The modified equations incorporate the Doppler shift  $kv\theta$ , where  $v$  is the velocity of the atom considered.

$$\ddot{E} + 2\gamma_c \dot{E} + (\omega_c - kv\theta)^2 E = \left( \frac{4\pi\omega_c^2}{V'} \right) p \quad (4.1)$$

$$\ddot{p} + 2\gamma_p \dot{p} + \omega^2 p = \left( \frac{2\mu^2 \omega}{\hbar} \right) E + 4\omega\mu\sqrt{N_u}G \quad (4.2)$$

The shift has been left out of the right side of the first equation because it is much smaller than an optical frequency and negligible in the way it enters the final result. It has also been assumed that  $\sin \theta \approx \theta$ . It would be of little value to write out the solution to these equations as a function of  $v$  and  $\theta$ , which would consist of replacing  $\omega_c$  by  $\omega_c - kv\theta$  and  $V$  by  $V'$  in Equations 2-17 through 2-20 and the included text. Since we cannot distinguish emission angle or atomic velocity in our experiments, these equations would also not be useful until included the velocity distribution and integrated over all included velocities and angles.

#### 4.2.1 Atom-Cavity Emission Lineshape

In measuring the normal mode splitting, the overall intensity is not important because all of the information is contained in the lineshape and corresponding frequencies. Therefore, the overall constants will be ignored in what follows. The spectral response (Equation 2.16), or power output as we tune the laser, can be expressed as the product of two Lorentzians (Equation 2.18). For weak coupling, one of the Lorentzians can be associated with the cavity for a given (positive or negative) detuning, and is Doppler broadened in accordance with earlier discussions, while the "atom Lorentzian" is not. To extract a measurable quantity from our mathematics, we should multiply this by the velocity distribution function and integrate over all velocities in the beam and all angles encompassed by the mirrors. For an unselected effusive beam, we have

$$P_\omega(\Omega) \propto \int_{-\sin \theta_{max}}^{\sin \theta_{max}} d(\sin \theta) \int_0^\infty dx x^2 e^{-x^2} \mathcal{L}_\pm(\Omega) \mathcal{L}_\mp(\Omega, x, \theta) \frac{1}{V'(x)} \quad (4.3)$$

It is not really necessary in the paraxial approximation to have included the sine functions, but this was done to emphasize that  $\theta$  has been defined as illustrated in Figure 4-1 rather than as the usual polar angle. Even for limiting cases, this expression is not easy

to integrate (except perhaps for low velocity atoms). At and near  $\theta = 0$  the Doppler effect does not apply, while at large angles there is a range of resonance frequencies corresponding to different velocities but whose strength is decreased by the length of the vertical cord of the mirrors which shrinks with increasing  $\theta$ . The computer does not need to simplify the calculus, and so a computer solution is presented in Sections 4.4 and 4.5.

### 4.3 Doppler Reduced Coupling

Section 4.1 discusses the loss of atom-cavity coupling due to the cavity Doppler effect. Now we will calculate that loss of coupling based on the theory that the reduced velocity dependent resonant area of the mirrors will translate into an increased mode volume because of the diffraction limited cavity mode waist. The concentric cavity mode volume is inversely proportional to the solid angle factor  $f = \frac{3}{4}\theta_{beam}^2$  introduced in Chapter 2. By calculating a reduced solid angle factor to account for the reduced coupling, we are assuming that the cavity Doppler effect will affect the coupling in a way similar to introducing an aperture so an atom can see less of the mirrors.

For this analysis, we consider an atom-cavity system in which the cavity is tuned to the free space atomic center frequency  $\omega$ . We will consider the atom-cavity system lineshape to be a function with a full width at half maximum of  $\gamma_c + \gamma_p$ , the width of the two convolved Lorentzians. Photons Doppler shifted within this frequency range are considered to couple the system, and those outside of it are considered lost. For atoms moving at velocities for which photons emitted at every angle of the mirrors are resonant, we will consider the atom-cavity coupling unaffected by the cavity Doppler effect. Thus the limit at which we start to modify the coupling is

$$\Omega \pm kv \sin \theta_{max} > \omega \pm (\gamma_c + \gamma_p) \quad (4.4)$$

Using the resonant assumption  $\Omega = \omega$ , the paraxial approximation  $\sin \theta \approx \theta$ , and the

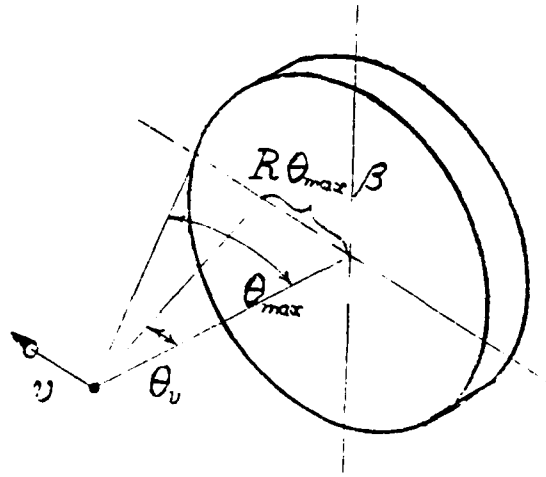


Figure 4-3: Notation for Calculating the Resonant Area of a Cavity Mirror

solid angle factor, the condition becomes

$$v > \frac{\gamma_c + \gamma_p}{k\theta_{max}} \quad (4.5)$$

$$\theta_{max} = \theta_{beam} = 2\sqrt{\frac{f}{3}} \quad (4.6)$$

In computing the resonant area of one of the mirrors, we will use the notation of Figure 4-3. The variable  $\theta_v$  is the velocity dependent angle which defines the limit of our resonant area

$$\theta_v = \frac{\gamma_c + \gamma_p}{kv} \quad (4.7)$$

The reduction in  $f$  is computed, as discussed earlier, by taking the ratio of the "resonant area" we have defined to the total mirror area. If we disregard the curvature of the mirrors, which we can do with a small enough solid angle subtended by the mirrors, the area of the full mirror surface is a circle, and straight vertical lines mark the resonance boundaries. The reduced area can be easily calculated if one divides the area within these boundaries into two slices of a circle and two triangles. Summing these sections and dividing by the area of the total circle, one arrives at the reduced solid angle factor

for an atom of velocity  $v$ , which is

$$\frac{V}{V'} = \frac{f'}{f} = \frac{2}{\pi} \left( \beta \sqrt{1 - \beta^2} + \arcsin \beta \right) \quad (4.8)$$

$$\beta = \frac{\sin \theta_v}{\theta_{max}} \quad (4.9)$$

This reduced coupling or increased mode volume should be included in Equation 4.3, after which the lineshape can be computed by integrating over all appropriate speeds and angles.

#### 4.4 Computer Solution to Doppler Modified Lineshape

The strong coupling limit does not lend itself to any obvious simplifications or approximations to make the integration over angles and velocities more tractable. A flowchart for a computer program which plots the spectral response lineshape which includes the Doppler shift and the reduced coupling is included at Appendix A. This algorithm includes the effective aperture function  $A(x)$  for a velocity selector and is integrated only over velocity selector allowed velocities. The integrations are done with Simpson's Rule or some other equal interval numerical integration method. The product of the Lorentzians used in the program is written in a less transparent form than in Equation 2.17, and uses several dimensionless parameters in addition to those dimensionless variables and parameters already defined: velocity  $x$ , solid angle factor  $f$ , finesse  $\mathcal{F}$ , selected velocity  $\alpha$ , reduced coupling factor  $\beta$  and velocity selector resolution  $\gamma$ . These new dimensionless parameters are

$$r = \frac{\gamma_c}{\gamma_p}, \Delta = \frac{\omega - \omega_c}{\gamma_p}, \delta = \frac{\Omega - \omega_c}{\gamma_p}$$

and angles modified by the factor  $ku_{th}/\gamma_p$

$$\Theta = \theta \frac{ku_{th}}{\gamma_p}, \Theta_{max} = 2\sqrt{\frac{f}{3}} \frac{ku_{th}}{\gamma_p}$$

The velocity limit for modifying the coupling is defined by the condition in Equations 4.5 and 4.6, but is included in the flowchart as the condition that  $\beta$  must not be greater than one. Written in terms of these dimensionless parameters, the program is well suited for evaluating the splitting requirements as the parameters are the ones controlled in the experiment.

## 4.5 Computer Generated Lineshapes

Figures 4-4 through 4-11 show the spectral response of the atom-cavity system as the exciting laser is tuned through the resonances for various values of the parameters  $\alpha$  and  $\gamma$ . The values of finesse,  $\gamma_p$ , and  $\gamma_c$  are values we believe we can achieve in future experiments. Figures 4-4 through 4-7 compare the lineshapes for descending values of  $\alpha$  for our current velocity selector. Figures 4-8 through 4-11 make a similar comparison for decreasing values of  $\gamma$  with  $\alpha$  fixed. The calculated density reduction from the velocity selector is written on each figure.

To continue this analysis, we will quantify the depth of the splitting by the contrast ratio, which is defined as the ratio of the signal intensity at the peaks to the local minimum between the peaks. For a system which can exhibit splitting, the splitting can be theoretically better resolved by lowering  $\alpha$ ,  $\gamma$ , or both, as illustrated in the figures. All of these actions decrease the density of atoms, which we have to balance against the improvement in contrast ratio. This is because, for a given counting time, the signal to noise ratio depends on the density of atoms, and the noise can inhibit the resolution of the lineshape.

The signal to noise ratio can be increased by counting each data point for a longer period, as discussed at the beginning of the next chapter. An adequate density is one

which allows us to measure the splitting with a “reasonable” count time, where “reasonable” loosely means that laser or cavity drift do not obscure the splitting and the experimenters are willing to do the experiment. A numerical analysis of this issue is included in Chapter 5; it uses the theory of this section and the density information of our velocity selector experiments.

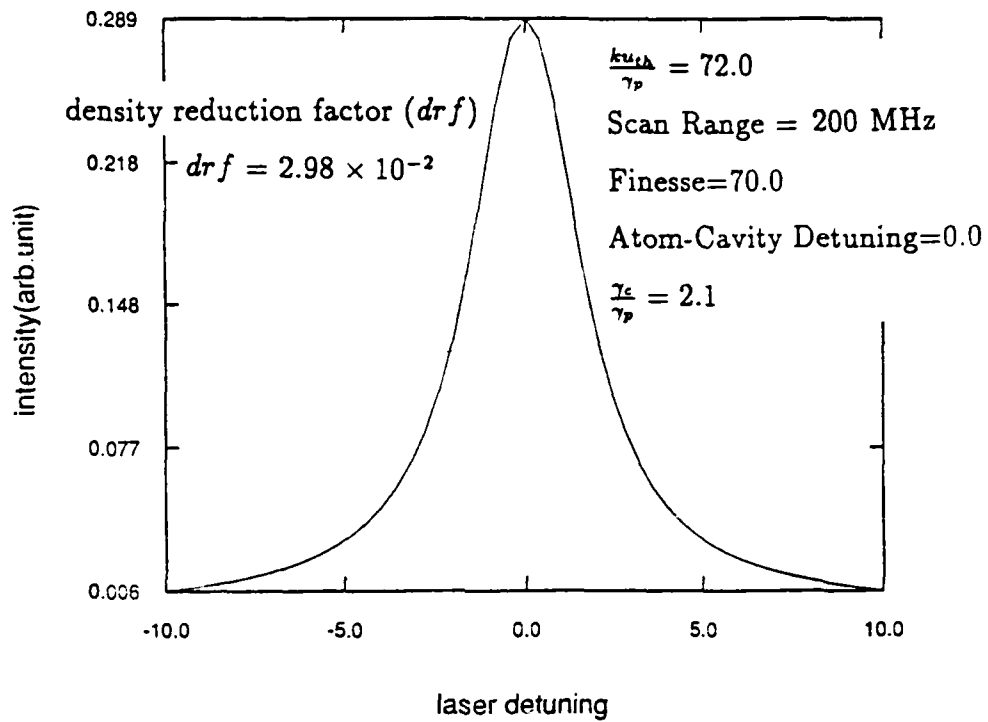


Figure 4-4: Theoretical Atom-Cavity Spectrum,  $\alpha = .40, \gamma = .44$

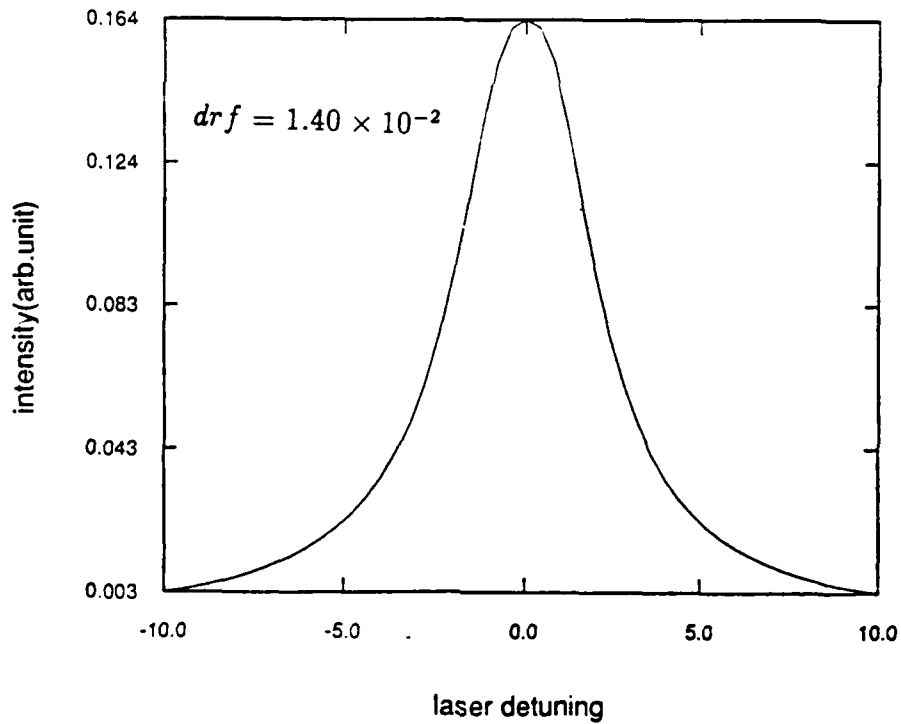


Figure 4-5: Theoretical Atom-Cavity Spectrum,  $\alpha = .30, \gamma = .44$

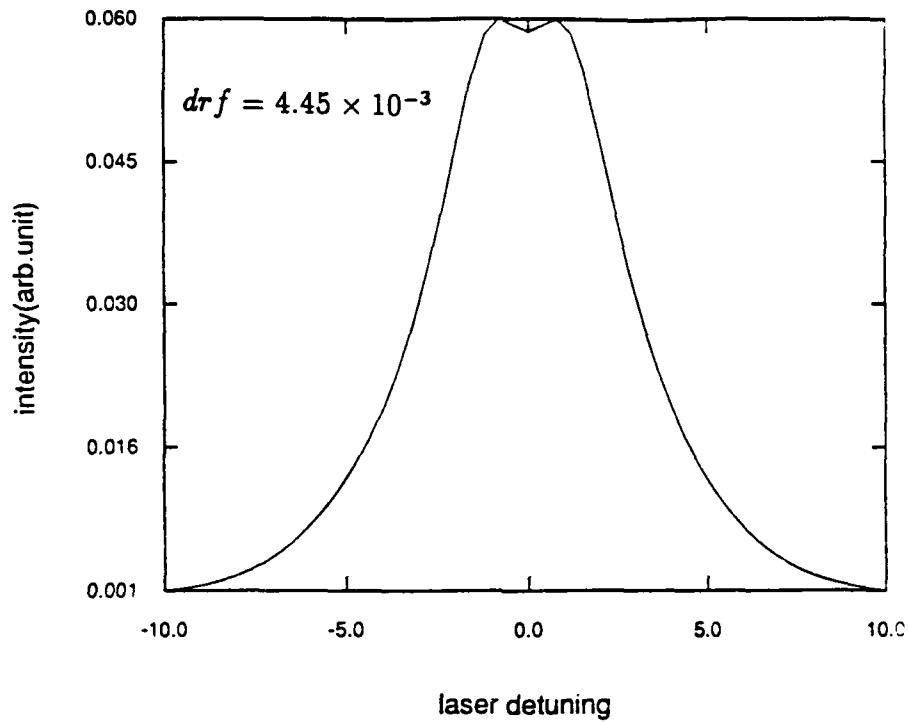


Figure 4-6: Theoretical Atom-Cavity Spectrum,  $\alpha = .20, \gamma = .44$

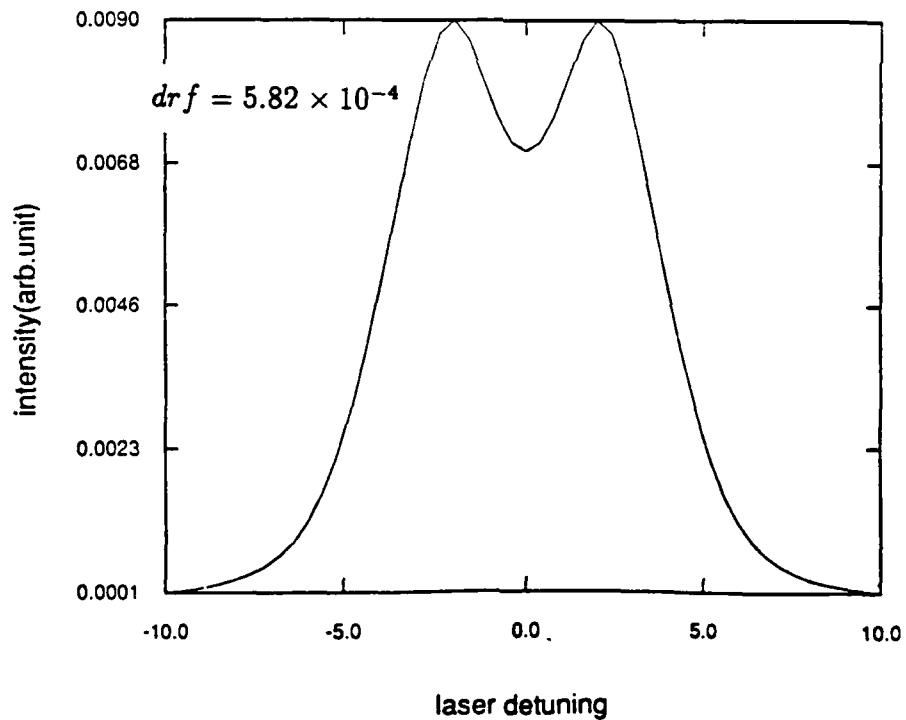


Figure 4-7: Theoretical Atom-Cavity Spectrum,  $\alpha = .10, \gamma = .44$

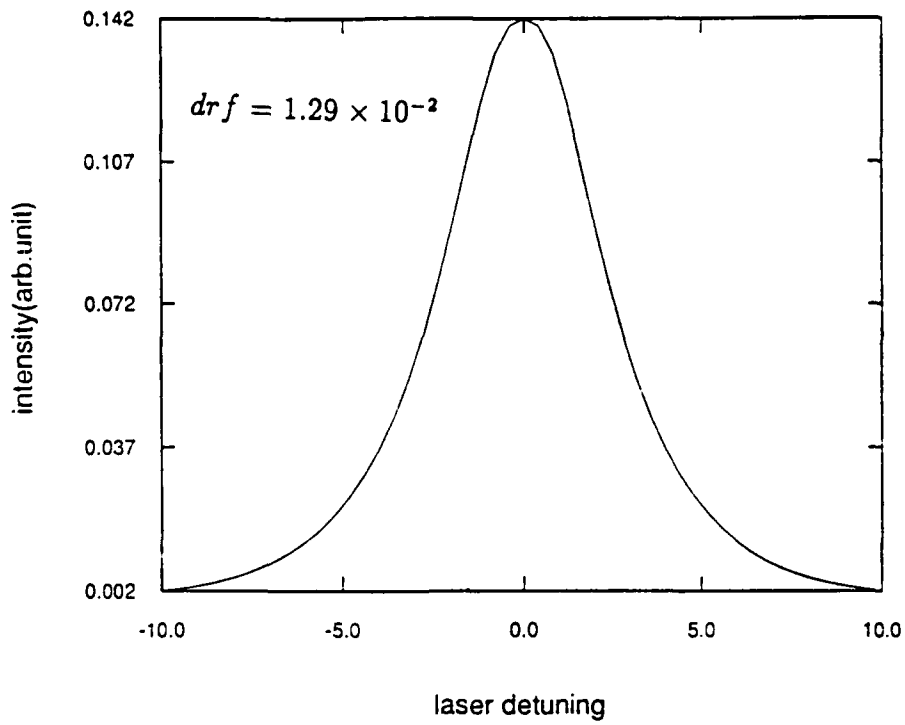


Figure 4-8: Theoretical Atom-Cavity Spectrum,  $\alpha = .15, \gamma = .80$

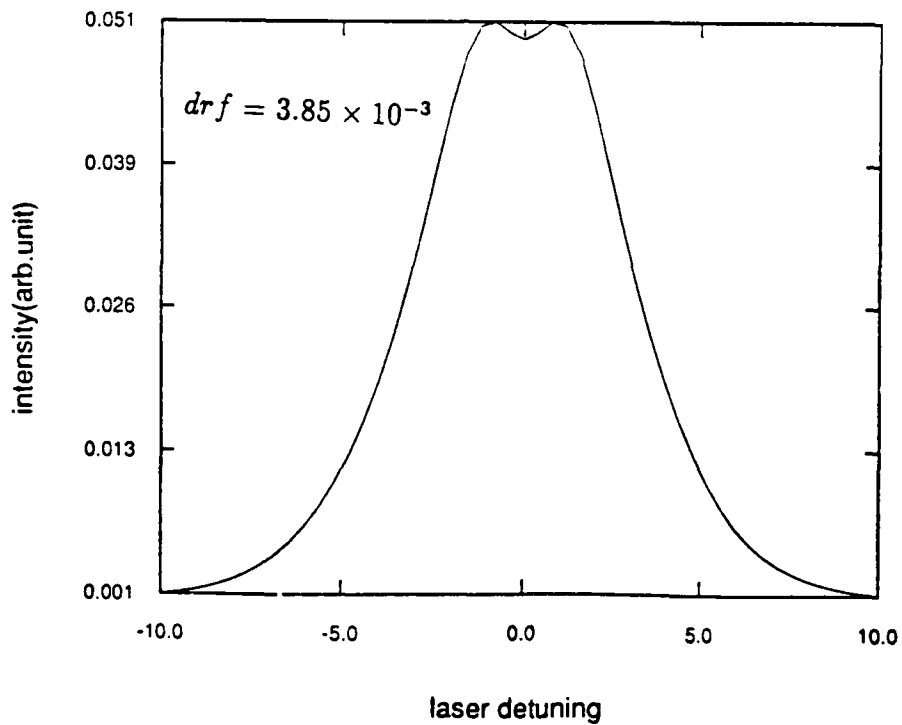


Figure 4-9: Theoretical Atom-Cavity Spectrum,  $\alpha = .15, \gamma = .60$

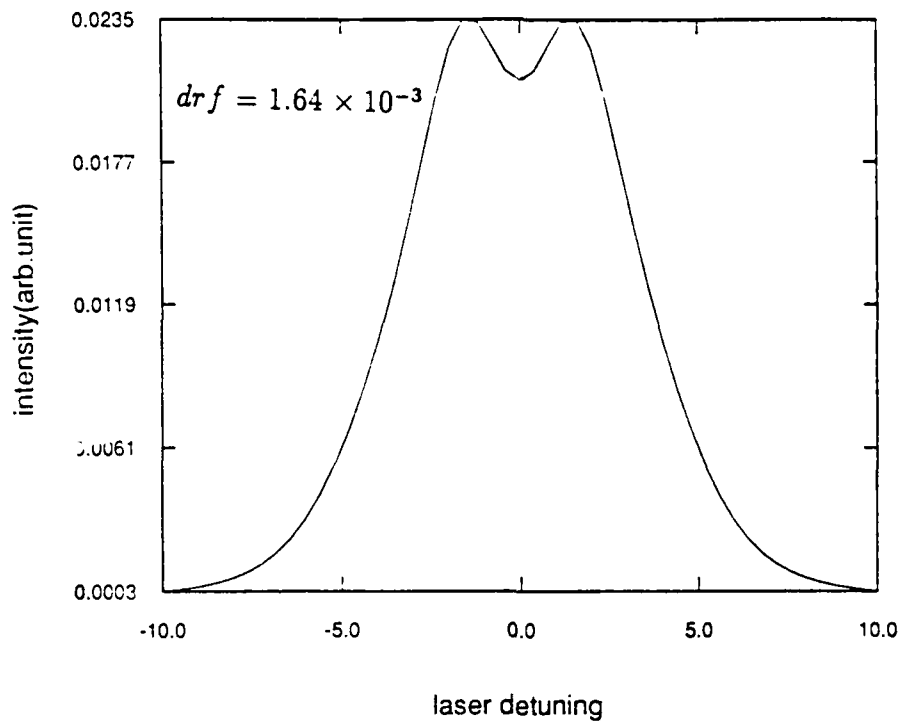


Figure 4-10: Theoretical Atom-Cavity Spectrum,  $\alpha = .15, \gamma = .40$

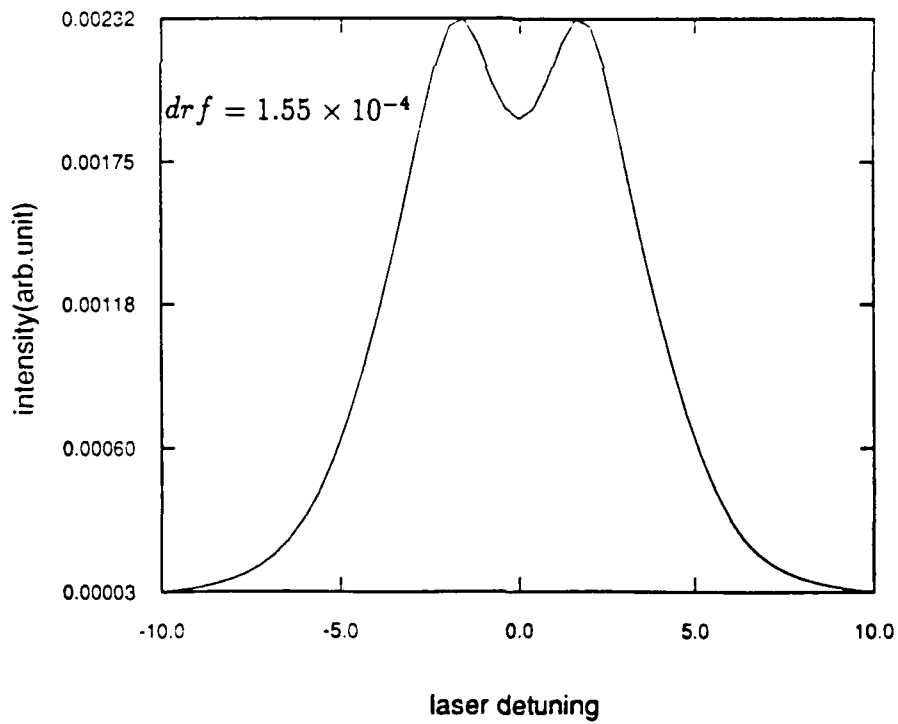


Figure 4-11: Theoretical Atom-Cavity Spectrum,  $\alpha = .15, \gamma = .05$

# Chapter 5

## Velocity Selection Experiments

### 5.1 Objectives

Two factors will determine whether we can use velocity selection to overcome the cavity Doppler effect limitation to measuring the single atom - optical cavity coupling: the resultant velocity distribution and the density of atoms. We ran experiments to determine these factors for various combinations of oven temperature and velocity selector speed. In doing so, we hoped to learn how well the theory presented in Chapter 3 predicts these factors and what additional losses are incurred. We also hoped to learn how well the velocity selector and associated equipment would function, how much vibration they would add, and their effect on maintaining a vacuum. Kyungwon An calculated the optimum oven aperture size and shape assuming it was necessary that the mean free path in the oven was longer than or equal to the shortest oven aperture dimension, a condition to keep us in the effusive beam limit. These experiments could help us decide whether this is the correct condition for attaining maximum density and at what temperature we deviate significantly from the Gaussian speed distribution on which our theory is based.

Because of irreducible noise in the atom-cavity experiments, primarily dark noise in the photomultiplier tubes of about 50 counts per second, it is necessary to have some minimum count rate to get a signal to noise ratio adequate for the contrast ratio of

the atom-cavity spectrum. Calling that signal to noise ratio  $X$  and assuming we can eliminate all other sources of noise, we have the condition

$$\left(\frac{\text{Signal}}{\text{Noise}}\right) = \frac{\text{Signal}}{\sqrt{\text{Signal} + \text{Background}}} = X \quad (5.1)$$

For a beam density  $n$ , interaction volume  $V_{\text{int}}$ , count time  $T$ , cavity efficiency  $\eta_1$ , and collection efficiency  $\eta_2$ , the cavity enhanced signal [14][p. 1320] collected over a solid angle  $f/2 = 3\Omega/16\pi$  (adjusted for the dipole radiation pattern) is

$$\text{Signal} = ST \quad (5.2)$$

$$S = \left(n \frac{\text{atoms}}{\text{cm}^3}\right) \left(\frac{1}{\tau} \frac{I}{2I_s} \frac{\text{photons}}{\text{atom sec}}\right) (V_{\text{int}} \text{cm}^3) \left(\eta_1 \eta_2 \frac{\text{counts}}{\text{photon}}\right) \left(\frac{f}{2}\right) \left(\frac{1}{1-R} \frac{\gamma_c}{\gamma_c + \gamma_p}\right) \quad (5.3)$$

With a background count rate  $B$ , the background is

$$\text{Background} = BT \quad (5.4)$$

Equation 5.1 is a quadratic equation in signal, which we can solve for the minimum beam density to achieve our minimum signal to noise ratio.

$$n = \left(\tau \frac{2I_s}{I}\right) \left(\frac{1}{V_{\text{int}} T \eta_1 \eta_2}\right) \left(\frac{2(1-R)\gamma_c + \gamma_p}{f \gamma_c}\right) \left[\frac{X^2}{2} \left(1 + \sqrt{1 + \frac{4BT}{X^2}}\right)\right] \quad (5.5)$$

By selecting a counting time per point  $T$  which is near the limit of being "reasonable" and estimating the necessary signal to noise ratio  $X$ , we can get a rough idea of minimum velocity selected densities needed to successfully run the experiment. The atomic lifetime  $\tau$  of barium is 8 nsec, a reasonable saturation parameter  $\frac{I}{I_s}$  is .2, the measured counting efficiency  $\eta_1$  is about .02, a reasonable cavity efficiency  $\eta_2$  is .3, and the interaction volume for a finesse of  $\mathcal{F} = 70$  is about  $10^{-9} \text{cm}^3$ . We can estimate the cavity enhancement of the signal into the solid angle proportional to  $f$  using an effective reflectivity. Since

$\mathcal{F} \approx \pi/(1 - R)$  for a reflectivity limited finesse, we have an effective reflectivity for a finesse of 70 ( $\gamma_c = 21$ ) which is  $R = (\mathcal{F} - \pi)/\mathcal{F} = (70 - \pi)/70 = 95.5\%$ . Thus the spontaneous emission into  $f$  is enhanced by approximately a factor of fifteen. Assuming we need a signal to noise ratio of five and can count 20 minutes per point, we would need a beam density of  $2.6 \times 10^4 \text{cm}^{-3}$ . If we can achieve this density in the interaction region for  $\alpha \approx .15$ , then the cavity Doppler effect should not be an impediment to seeing the splitting.

Finally, these experiments should help us better determine what needs to be changed in the laboratory before we go into velocity selected atom-cavity experiments. We designed much of the equipment in the velocity selection experiments to conveniently fit our current vacuum chamber and resonator with minimum modifications. The velocity selection experiments could help us decide which of those convenient and economical choices, such as placing the motor inside the vacuum, will have to be abandoned.

## 5.2 Conduct of the Experiments

Figure 5-1 is a schematic illustration of the velocity selector experiment. Two types of fluorescence measurements gave us the desired information about the velocity profile and the atomic beam density: fluorescence from a nearly counterpropagating beam which we call the Doppler beam, and fluorescence from an orthogonal beam which we call the C-beam. For both beams, data was taken both with and without the velocity selector, allowing us to evaluate the effect of the velocity selector. The signal in each case was acquired as a Coherent Model 699 ring dye laser scanned through the fluorescence profile while a camera lens and other optical elements focused the light into a photomultiplier tube. The electrical signal of the photomultiplier was stored by a personal computer connected to a photon counter, which collected 500 data points at 200 msec/point. A perpendicular reference beam was also collected through an optical fiber bundle and then through a voltmeter connected to the computer.

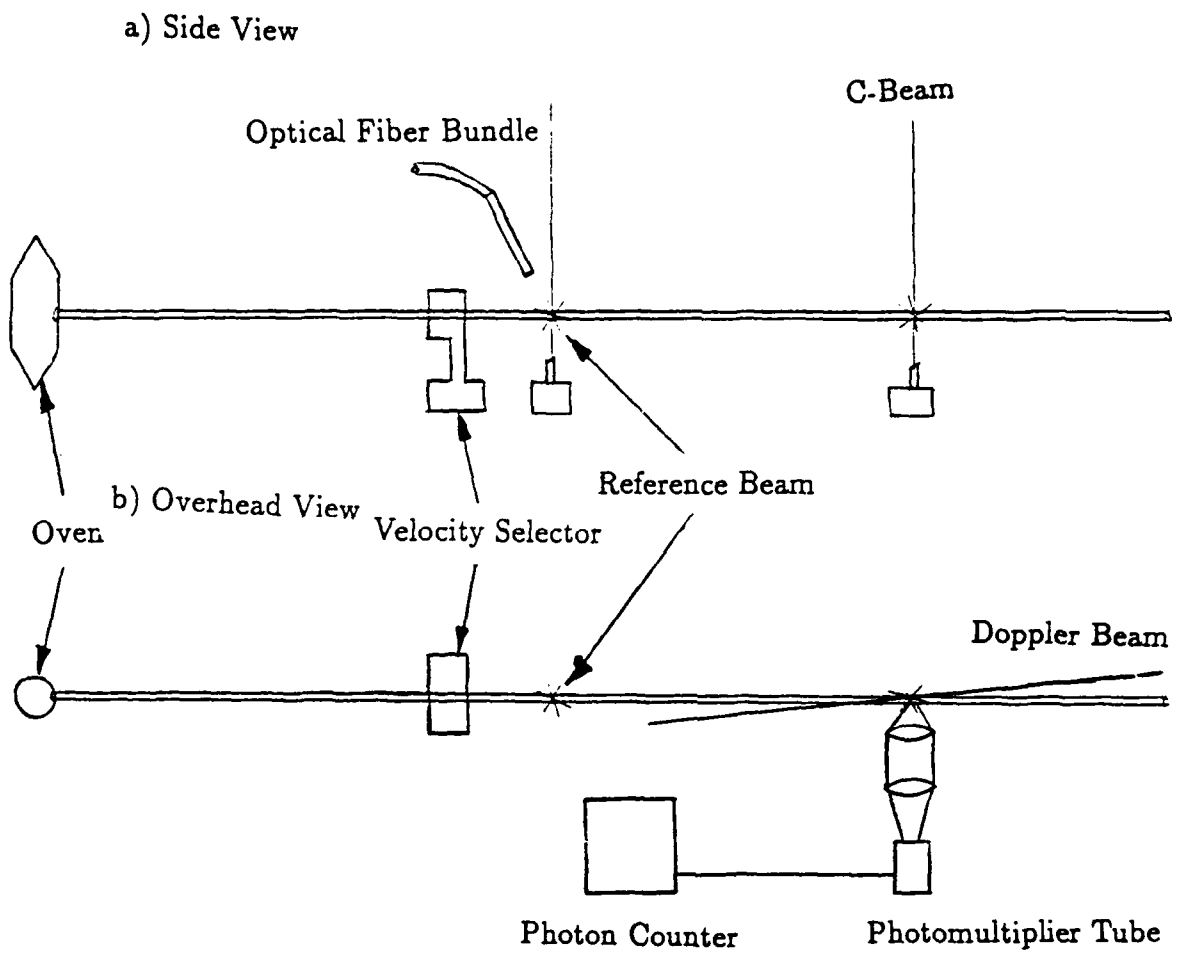


Figure 5-1: Schematic of Velocity Selector Experiment

### 5.2.1 Interpreting the Data

The data from the C-beam measurements is the most straightforward to interpret and gives stronger signals at low atomic densities, but it does not give us any information on the velocity profile. The C-beam signal has a Lorentzian lineshape, slightly Doppler broadened because of misalignment or beam divergence from a natural linewidth of 20 MHz to about 30 MHz. Density reduction could be computed by comparing the integrated counts of a selected beam to the integrated counts of an unselected beam, but the integration is not really necessary. Since the lineshape of all signals, velocity selected and unselected, is the same, the ratio of the height of a velocity selected signal to the height of an unselected signal gives the density reduction, assuming the atomic and laser beams maintain a constant strength. This assumption, however, cannot be taken for granted, as it accounts for most of the experimental uncertainty.

Doppler beam measurements contain information on both the distribution of atoms and their total density. An atom of velocity  $\vec{v}$  sees the exciting laser beam shifted by  $\vec{k} \cdot \vec{v}$ . While this shift is essentially zero for the C-beam, it amounts to a red shift of magnitude  $kv$  for an atom in the Doppler beam. Since the atomic linewidth is less than 3% of the width of the Gaussian speed distribution for any reasonable oven temperature, and the laser bandwidth is another order of magnitude smaller, the intensity of the radiation as we scan the laser will be in proportion to the number of atoms Doppler shifted into resonance. The lineshape will mirror the velocity distribution of the atomic beam. Since we collect a reference signal from a perpendicular beam, we know what frequency in the scan we can associate with zero velocity atoms to within the small Doppler shift of the reference beam. On some of the Doppler beam scans, the C-beam was inserted, and it also marks the zero velocity atoms.

The Doppler beam plots display two other effects that at first confused us. In addition to the velocity profile, we see a mirror image peak which is blue shifted and much smaller than the red shifted signal. This can be attributed to the reflection of the Doppler beam off the last atomic beam aperture. As this aperture also contributed a lot to

the background because of scattering, we removed it in our last set of data. We also saw an apparent increase in very slow atom ( $v < 0.1u_{th}$ ) density as we increased oven temperature, even as the beam became more and more supersonic. We now believe this to be attributable to isotopes of Barium moving at some non-zero velocity that are resonant at higher frequencies and are Doppler shifted into resonance at the same frequencies we associate with the very slow  $^{138}\text{Ba}$  atoms. On the scale of the plots included in this thesis, this effect is not visible.

### 5.2.2 Controlling the Environment

Perhaps the biggest challenge in collecting the data was to control the environment well enough to allow us to make valid comparisons of data collected from several minutes up to an hour apart. To compute density reduction in particular, we needed to compare a selected and an unselected run, which could not be made simultaneously of course. Furthermore, it was impractical to collect an unselected profile for every selected profile because of the time needed to adjust the velocity selector height and, more significantly, because we would introduce even more uncertainty into the comparison of consecutive runs. Most of our effort during data collection was monitoring and adjusting the laser power, the oven current, the vacuum chamber pressure, the atomic beam alignment, and the velocity selector speed.

The laser power tends to drop and the laser becomes less stable as it drifts out of alignment and as it nears the end of the lifetime of the dye. It is particularly troublesome when the laser hops to a different frequency during a scan. The only remedy for these problems is to realign the laser and replace the dye when necessary. There is, however, a tendency for the frequency and power to fluctuate somewhat regardless of how well the laser is operating. By applying a correction factor based on the signal strength of the reference beam, we fairly well compensated for this variation. Because of space limitations, our reference laser beam intersected the atomic beam after the velocity selector, which did somewhat limit the accuracy of this correction factor.

A second variable can also affect the reference beam signal strength. Since the temperature of the oven fluctuates, we expect a fluctuation in the atomic beam density. We have been unable to spot weld or otherwise permanently attach our thermocouple wire to the tantulum oven to get a temperature reading. The oven current is related to the temperature, so we have substituted a current reading for a temperature reading. The problem with this is that the ammeter is not nearly as precise as a thermocouple, and the reading is probably less accurate than the temperature as measured by the Doppler shift. This assertion is evidenced by the fact that we have two data runs at 210 Amps, one of which shows an effusive beam while the other is clearly supersonic. Assuming the atomic density did vary, we have compensated for it with the change in signal strength of the reference beam signal, but if the velocity distribution has also changed significantly our comparisons may not be completely valid.

The vacuum chamber pressure has presented some unexpected problems. We did expect, and did experience, some problems with outgassing as we tried to damp out vibrations. But we also saw a pressure rise associated with running the velocity selector, which at first we also associated with outgassing. Without running the velocity selector, we were reaching a steady state pressure of around  $5 \times 10^{-6}$  to  $1 \times 10^{-5}$  torr. With the original motor, the pressure seemed to rise rapidly when the velocity selector was turning at high speed. We purchased a new motor which can only rotate at half the maximum speed of the old motor, 400 Hz, but is much quieter. We do, however, still see what appears to be a "leakage resonance" for the cavity at around 100 Hz, where the pressure rapidly rises to values exceeding  $2 \times 10^{-5}$  torr, probably associated with the o-rings on the feedthroughs to the translation stage and cooling lines. At these higher pressures, the signal is significantly attenuated.

In order to determine the maximum densities we can achieve, we must have the atomic beam and exciting laser beams properly aligned. Although we have the necessary controls to adjust the oven, the velocity selector, the lasers, and the smallest aperture, it is not always obvious when the system has drifted out of alignment. Based on the data,

this does not seem to be a significant problem, but it might have contributed to loss of density in some cases.

Velocity selector speed is determined in two ways. The velocity selector has a small piece of glass on the shaft which reflects either part of the Doppler beam or an inserted He-Ne laser beam into the reference beam optical fiber bundle. This produces a modulation at the frequency of the velocity selector, which we measure on an oscilloscope. In addition, the motor will generally run at half the input electrical frequency; since it is a synchronous motor, it will not operate well at any other rate. We can infer the velocity selector speed from this if we stay well within the range of frequencies supported by a particular capacitor. Since the velocity selector speed is such an important parameter, the direct measurement is preferred.

## 5.3 Fitting Doppler Profiles

The representative plots on the next five pages each have a velocity selected profile overlaying an unselected profile, both with theoretical fits. The first four are included in order of decreasing  $\alpha$ , and all are labeled with the oven current  $I_o$ , fitted thermal (most probable) velocity  $u_{th}$ ,  $\alpha$ , and the misalignment multiplier. The reference beam signal is used as a frequency marker to align the two plots. Both data runs are plotted on the same vertical scale, which is counts per 200 msec. The horizontal scale is the data point number; each of the 500 points represents the 8 MHz frequency scan of the exciting laser during a single collection period. The total scan range of each plot is 4 GHz. Background has been subtracted out.

### 5.3.1 Unselected Profiles

The fits for the unselected profiles fall into two distinct categories: those that fit the Gaussian speed distribution very well (like Figures 5-2 and 5-3), and those that are noticeably narrower (like Figures 5-4 and 5-5). As the oven temperature is increased, the

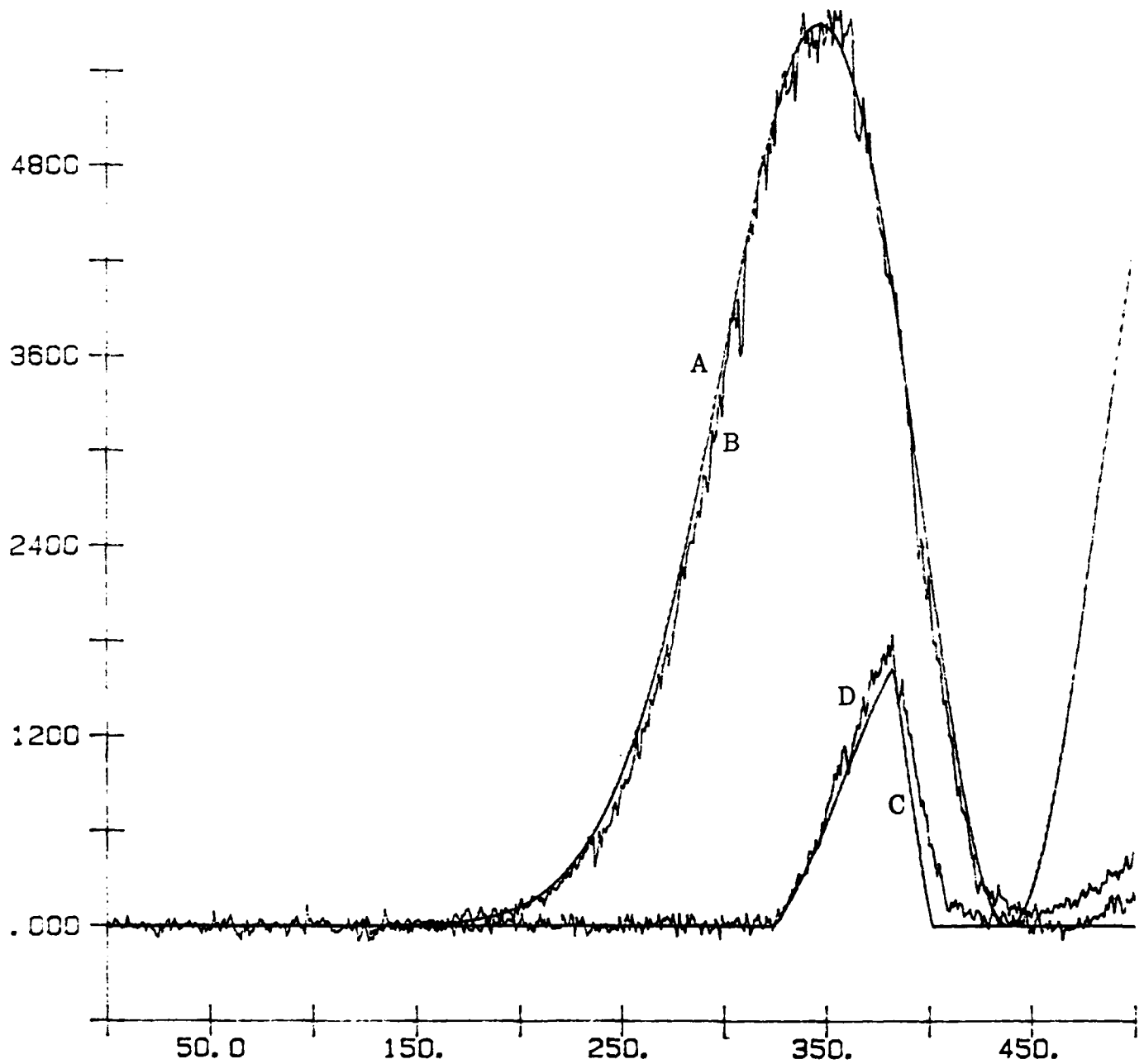


Figure 5-2: Doppler Beam Plot:  $I_o = 210 A$ ,  $u_{th} = 4.1 \times 10^4 \frac{cm}{sec}$ ,  $\alpha = .53$ ,  $\alpha$  and  $\gamma$  multiplied by 1.15 for misalignment. The curve labeled A is the Gaussian speed distribution, B is the Doppler profile without a velocity selector, C is the theoretical profile of the velocity selected beam given the measured quantities and assumed misalignment above, D is the velocity selected data.

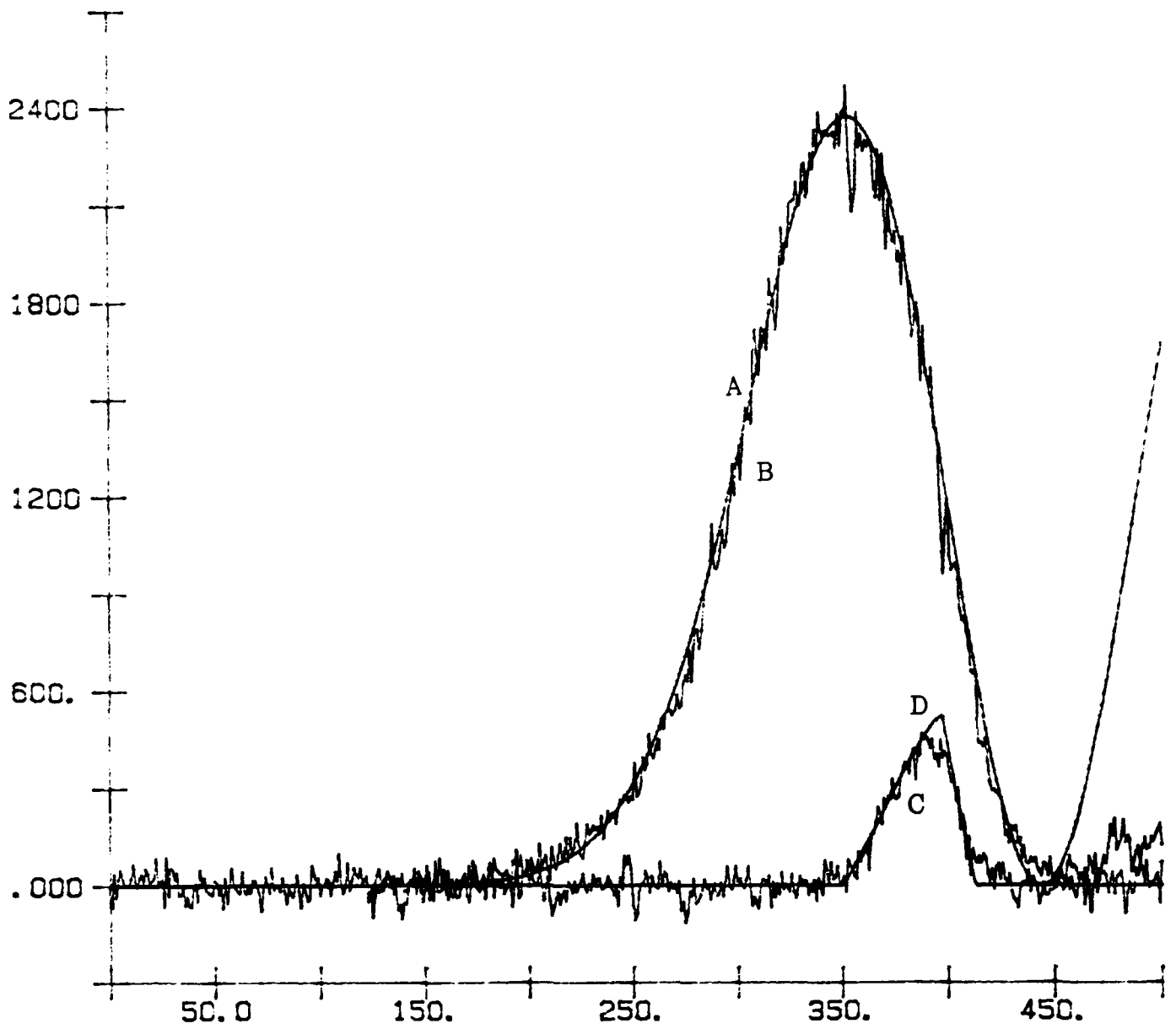


Figure 5-3: Doppler Beam Plot:  $I_o = 210 A$ ,  $u_{th} = 4.0 \times 10^4 \frac{cm}{sec}$ ,  $\alpha = .44$ ,  $\alpha$  and  $\gamma$  multiplied by 1.15 for misalignment. Curves explained in Figure 5-2

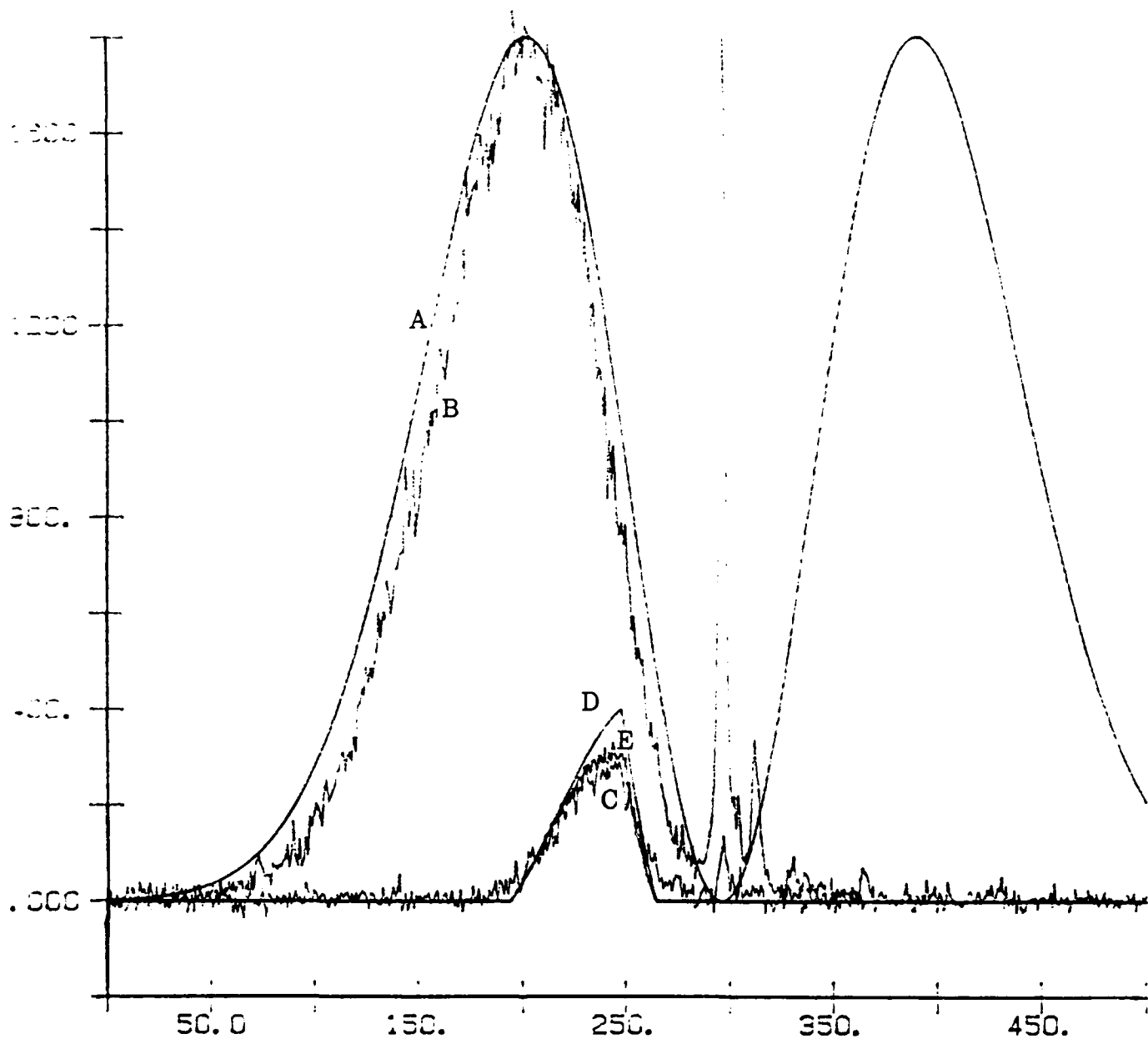


Figure 5-4: Doppler Beam Plot:  $I_o = 210 A$ ,  $u_{th} = 4.2 \times 10^4 \frac{cm}{sec}$ ,  $\alpha = .42$ ,  $\alpha$  and  $\gamma$  multiplied by 1.2 for misalignment. The sharp peak is the C-Beam and should be ignored. Curves are explained in Figure 5-2 except for E, which is the velocity selector function multiplied by the experimental speed distribution of B rather than the theoretical A.

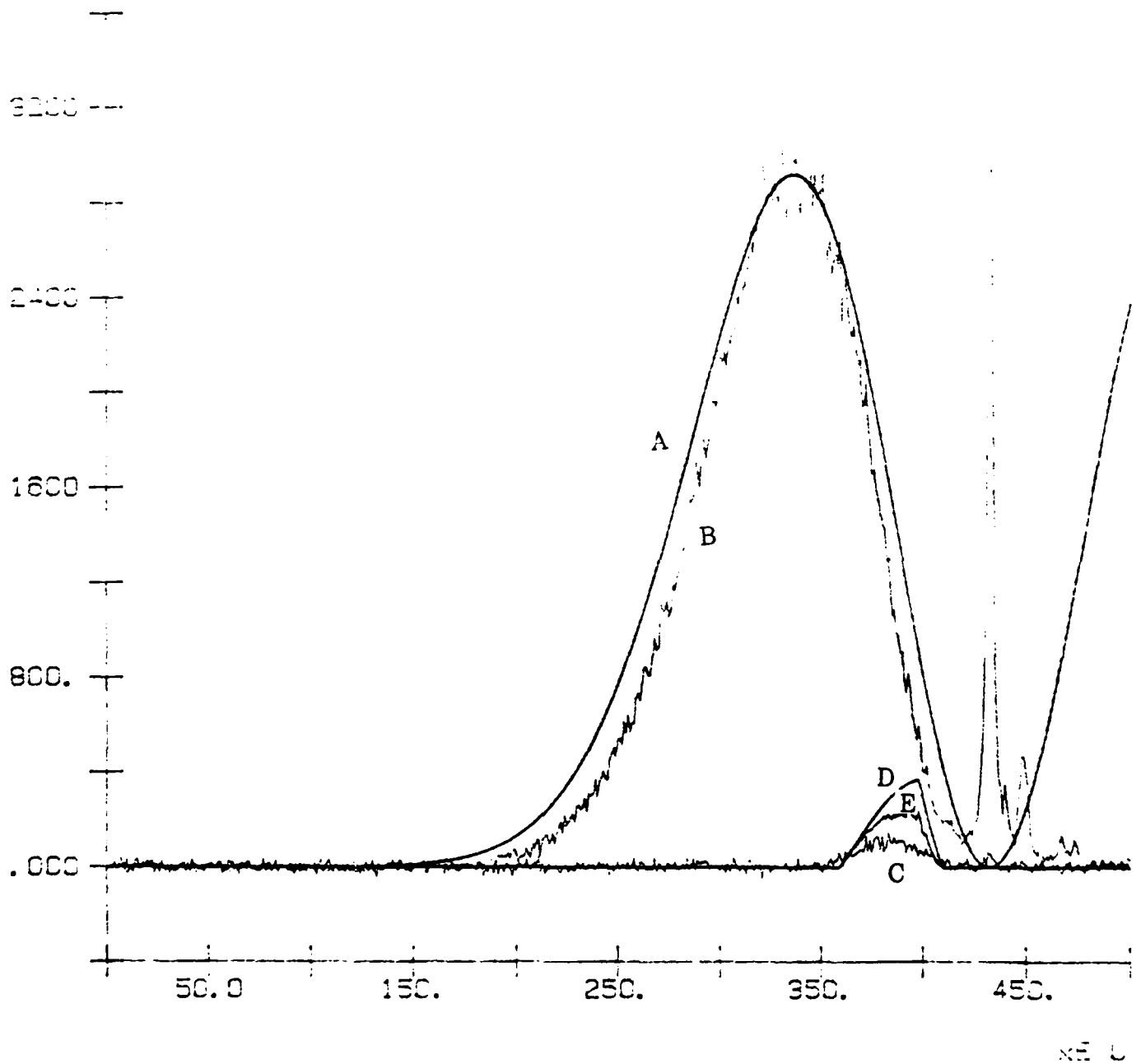


Figure 5-5: Doppler Beam Plot:  $I_0 = 225 A$ ,  $u_{th} = 4.25 \times 10^4 \frac{cm}{sec}$ ,  $\alpha = .30$ ,  $\alpha$  and  $\gamma$  multiplied by 1.2 for misalignment. The sharp peak is the C-Beam and should be ignored. Curves are explained in Figures 5-2 and 5-4.

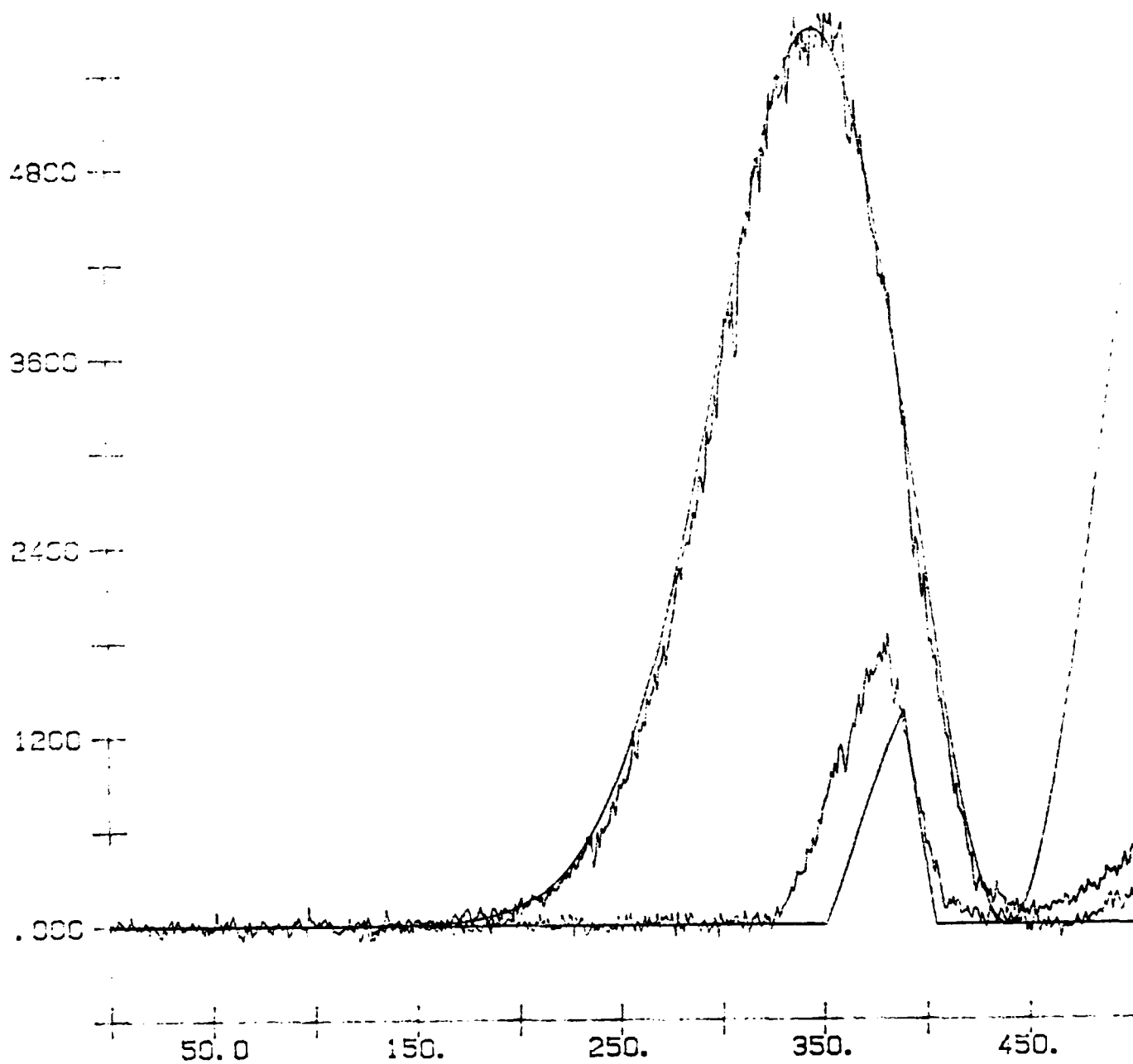


Figure 5-6: The same plot as Figure 5-2, but fit without adjusting  $\alpha$  and  $\gamma$  for misalignment.

mean free path of an atom in the oven decreases. When the mean free path is smaller than the oven aperture, collisions will occur in the vicinity of the aperture. Kinetic energy tends to equilibrate somewhat by these collisions and the beam becomes more directional while the velocity distribution becomes more monoenergetic. This is characteristic of supersonic flow, and, for our oven, the transition from effusive to supersonic flow occurs around 210 amps.

The curves labeled "B" are data from runs without the velocity selector, and the curves labeled "A" are the fits of the Gaussian speed distribution  $x^2 e^{-x^2}$  where  $x = v_0/u_{th}$ . These fits were made so that thermal velocity ( $u_{th} = \sqrt{2kT/M}$ ) was determined by the Doppler shift of the most probable velocity in the data, and the peak value was scaled to the data.

### 5.3.2 Misalignment

The misalignment of the velocity selector relative to the atomic beam is crucial to interpreting the fits to the velocity selected data. Based on our measured velocity selector parameter  $\gamma$  and velocity selector speed  $\alpha$ , the densities were too high and the peak of the selected curve was at too high of velocity. Since we can measure the velocity selector speed directly, our uncertainty in that measurement was only about 5%, which was limited only by our ability to read the oscilloscope. We measured the resolution,  $\gamma$ , to be .44 and certainly no greater than .50, yet this did not agree with the data. It was only when we included misalignment that these measured values agreed. The reason that misalignment had such an effect is that the length of our velocity selector is only about  $\frac{1}{4}$  inch, which means the velocity selector angle  $\phi_0$  of Figure 3-1 can be significantly changed by misalignment. Both  $\alpha$  and  $\gamma$  are inversely proportional to this angle.

The effect of misalignment can be easily understood with a two dimensional picture as shown in Figure 5-7. In this picture, the radius at which the beam intersects the velocity selector is "unrolled" into a plane so we see the "footprint" of the velocity selector. The angle  $\psi$  of Figure 5-7 is related to  $\phi_0$  by the relation  $\phi_0 = L \tan \psi / r_0$ . The angle  $\psi$  is

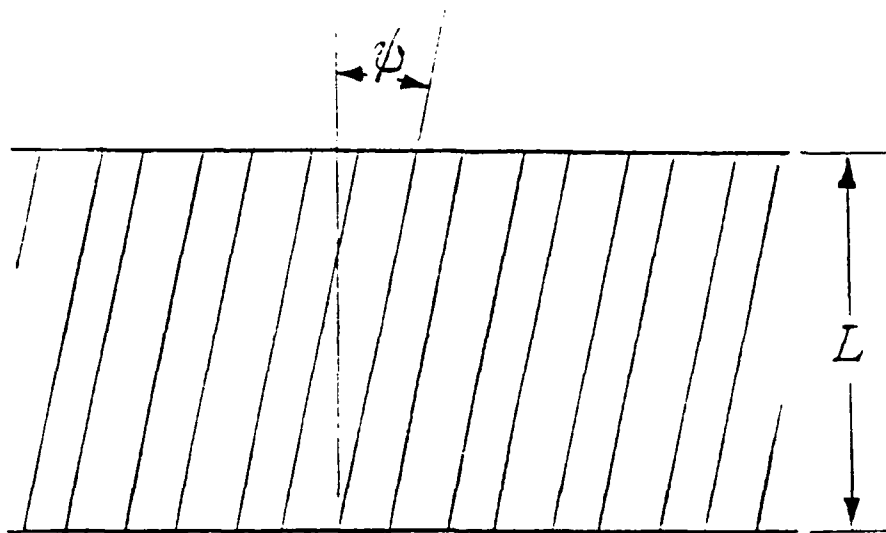


Figure 5-7: Two Dimensional Representation of the Velocity Selector

measured to be  $11.9^\circ$  within a standard deviation of the mean of  $.5^\circ$ . If the velocity selector is misaligned by  $1.5^\circ$ , both  $\alpha$  and  $\gamma$  will be increased by 15%.

From Chapter 3 we know that the maximum and minimum velocities allowed by the velocity selector are  $x_{max} = \alpha/(1 - \gamma)$  and  $x_{min} = \alpha/(1 + \gamma)$ . It is difficult to imagine how a significant number of atoms outside of this range could intersect the exciting laser. It is also unreasonable to expect that we could achieve higher densities than predicted by our simple theory. If we assume a misalignment of 15% for one experimental run and 20% for the other, the data fits the theory well. If we assume no misalignment, the range of selected velocities is much too small and the density is increased over theory in excess of probable experimental error. Figure 5-6 shows the fit of Figure 5-2 when misalignment is *not* assumed. All other plots assume the appropriate 13% or 17% decrease in  $\phi_0$  due to misalignment.

A misalignment of this size is certainly believable. There is a window on the vacuum chamber which stops the barium atoms that made it through the interaction region. The spot caused by these atoms is off center by roughly .5 cm in the direction which would decrease  $\psi$ . This is an atomic beam misalignment of nearly a degree. The vacuum

chamber itself does not have many good visual references for alignment, and another degree of misalignment could have easily been added.

The solution to prevent this in the future is not difficult. The oven hole and apertures provide references to align a He-Ne laser along the atomic beam path. A piece of reflecting glass stuck on the vertical face of the velocity selector can reflect this beam, and the velocity selector can be adjusted until the beam reflects back upon itself.

### 5.3.3 Selected Profiles

The selected profiles are labeled "C" in Figures 5-2 to 5-5. They are fit to a theoretical curve "D" which is derived from multiplying the effective aperture function  $A(x)$  by the Gaussian speed distribution. In the cases where the unselected distribution is supersonic (Figures 5-4 and 5-5), another theoretical fit labeled "E" is also included, in which the each data point for the unselected profile is multiplied by the effective aperture function. The fits are very good for when the beam is effusive as in Figures 5-2 and 5-3. For supersonic beams and high  $\alpha$ , most of the density reduction that cannot be attributed to the theory can be attributed to the velocity narrowing of the supersonic beam. We know this because curve "E" shows a good fit as in Figure 5-4. As we select slower atoms, there is an additional density reduction evident in Figure 5-3 and in all the supersonic data. We cannot say with confidence that this same reduction occurs for the effusive beam because the signal at those temperatures did not exceed noise at low  $\alpha$ . The magnitude of this reduction is evaluated in the next section. In all cases there is agreement to within 10% on the maximum and minimum selected velocities, which is evidence that we have correctly incorporated misalignment to within experimental error.

## 5.4 Density Reduction

Density reduction data is derived by taking the ratio of the areas under the Doppler curves and also by taking the ratio of the peak C-beam intensities. The density reduction factor

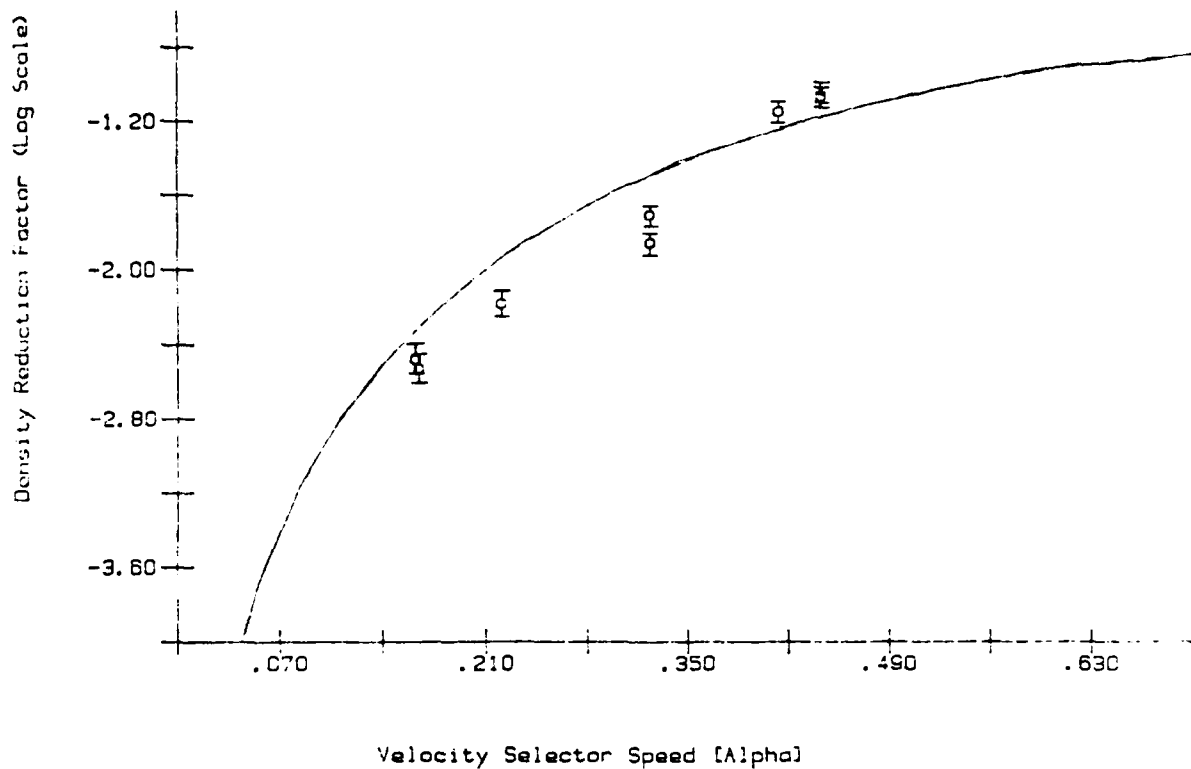


Figure 5-8: Density Reduction for an Effusive Beam at 210 Amps

is plotted against the selected velocity  $\alpha$  in Figures 5-8, 5-9, and 5-10. Each of the graphs corresponds to a different oven temperature. The theoretical curve is from Equation 3.14, assuming a misalignment which increases  $\alpha$  and  $\gamma$  by the appropriate 15 or 20 percent as discussed earlier.

At high values of  $\alpha$  the density reduction observed is in accordance with Equation 3.14 to within experimental error. As  $\alpha$  is decreased, however, there is roughly an additional loss of density which is about 50% for data at  $\alpha = .2$ . Based on an examination of Figure 5-5 and other data for supersonic beams, about half of that reduction might be attributed to the velocity narrowing in a supersonic beam. We know that the mean free path of the atoms in the vacuum chamber is much longer than the dimensions of the chamber at experimental pressures, so the additional loss is probably not due to collisions with background gasses.

A tentative hypothesis is that the loss is due to collisions near the velocity selector as some type of localized cloud of atoms forms from the large number of atoms not selected. The loss increases with decreasing velocity as we might expect for collisions. Perhaps

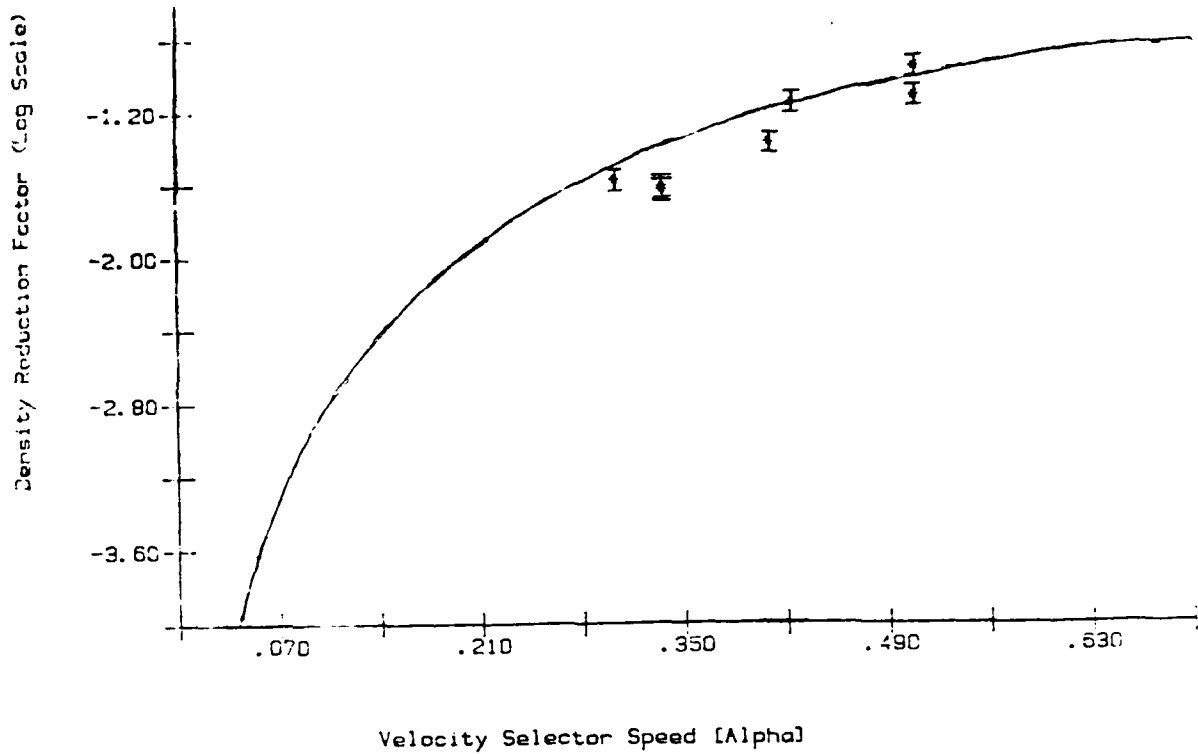


Figure 5-9: Density Reduction for a Supersonic Beam at 210 Amps

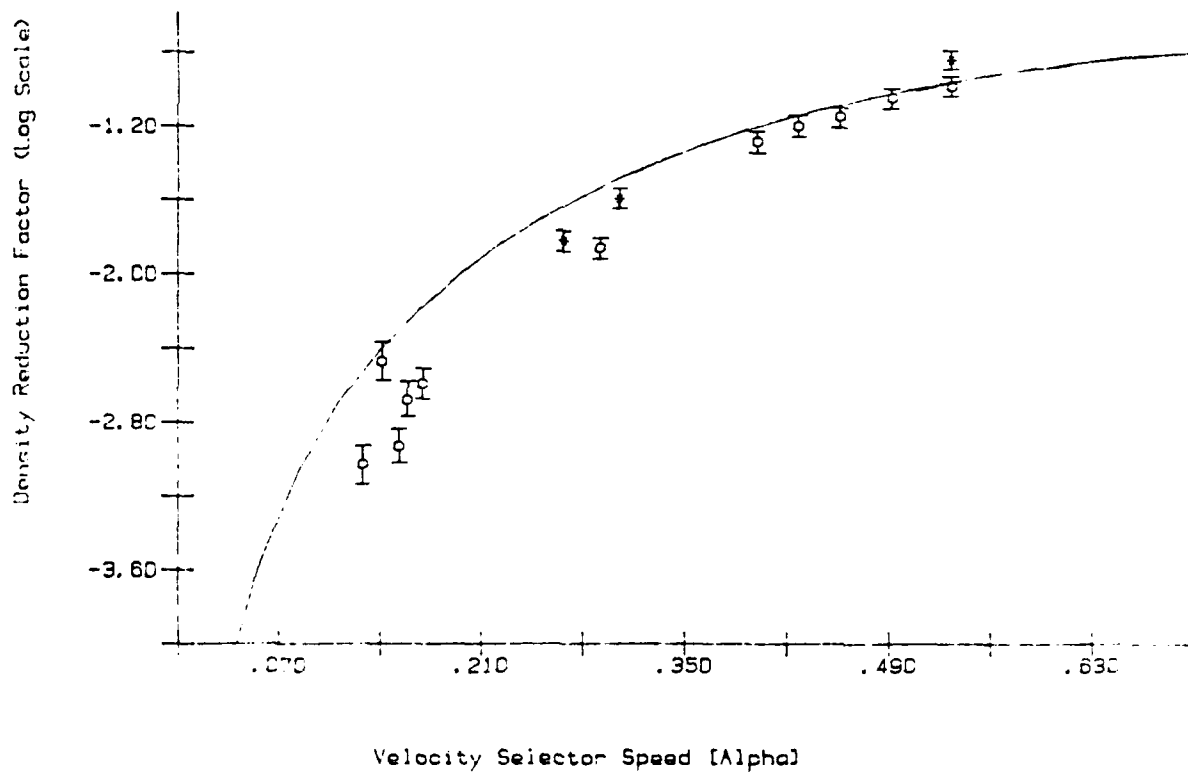


Figure 5-10: Density Reduction for a Supersonic Beam at 225 Amps

as atoms accumulate in the channels, the atoms which collide with the velocity selector groove walls knock other atoms out which can collide with atoms passing through.

## 5.5 Error Analysis

Statistical methods are not useful in estimating errors that arise from non-random fluctuations. Two critical pieces of equipment in our experiment tended to show such behavior over the several hours it took to acquire data: the oven and the laser. Both tend to decay in power over time, the oven current at a faster rate than the laser. As the laser drifts out of alignment, not only does the power go down, but the beam itself can shift. Despite this, decay in laser power actually seems to be negligible, although it is not clear whether all the decay observed in the reference beam signal was due to the oven. More troublesome was the current to the oven, since a small change in current translated into a large change in density.

During the conduct of the experiments, we constantly monitored the oven current and tried to keep it at a constant value for a number of runs. In analyzing the data, the velocity selected data was always compared to unselected data collected as close in time to it as practical. These procedures should have minimized the uncertainty introduced into the data. There was one occasion when it appears the oven temperature changed drastically during a run. We noticed a large drop in signal which we attributed to a significant rise in pressure as we were collecting data at the "leakage resonance". An unselected profile was collected after the pressure was back in an acceptable range, but it is nearly an order of magnitude too small to associate with the previous selected data, and the peak does not seem to be Doppler shifted enough to account for its profile shape. This suggests that important deviations may have occurred on other runs that were not so obvious. But we see that the data does not exhibit any correlation of density reduction to the order of data acquisition, so this concern does not appear to be justified. Our best estimate of the statistical variance of the data then is probably the deviation of the data

from a fitted curve, appropriate for random fluctuations.

There are several sources of experimental uncertainty that we can calculate. Since density reduction is a strong function of both  $\alpha$  and  $\gamma$ , it is important to reduce the uncertainty associated with those values. By accurately measuring  $\psi$ ,  $L$ ,  $l$ , and  $r_0$  we calculated a value for  $\gamma$  of  $.44 \pm .02$ . We measured the velocity selector speed once per run with an instrumental precision of about 5%. The misalignment can be extracted from the fits to about 3%, raising the total uncertainty in  $\alpha$  of about 6%. Thermal velocity is measured from the unselected Doppler beam profiles. The Doppler shift can be pinpointed within a spread of about 5 bins or 40 MHz. This is an uncertainty of about 5% which raises the uncertainty in  $\alpha$  now to about 8%. The counting process is described by Poissonian statistics, so the statistical variance in estimating density reduction from the C-beam signal is  $1/\sqrt{N}$ , where  $N$  is the number of counts for the selected beam peak. The statistical variance in the integrated area under the Doppler plots is negligible, assuming the background to be correctly subtracted. By ascribing all these uncertainties to the dependent variable, the density reduction factor, we can include them as error bars on the graphs of Figures 5-8, 5-9, and 5-10. The sources of uncertainty which we could not estimate well, oven current and laser power, are not included in the error bars although they are probably important in the actual experimental variance.

## 5.6 Absolute Density Estimate

We will soon undertake experiments to better determine the absolute density, because our interaction volume is somewhat uncertain. Since the interaction volume is partially defined by the focus of the camera lens, it is possible that we have not correctly estimated this volume. There does seem to be some consistency, however, in the estimate of oven density from data which fits the Maxwell-Boltzmann speed distribution and the expected oven density at the effusive limit. Using Equation 5.3 without the cavity enhancement, we can compute the atomic density from the peak C-beam count rate, since all of the

atoms are resonant at that frequency.

A calculation from one set of data is representative. The C-beam has a measured width ( $1/e$  point) of .003 cm for one axis and .0022 cm for the other. The image is apertured at the PMT so that the other dimension is also .003 cm. This gives us a saturation power of  $(30 \frac{\text{mW}}{\text{cm}^2})(6 \times 10^{-6} \text{cm}^2) = .18 \mu\text{W}$  and an interaction volume of  $2 \times 10^{-8} \text{cm}^3$ . This C-beam in this case weakly saturates the atomic beam. Putting these numbers in Equation 5.3 with  $\tau = 8$  nsec,  $\eta_1 = 1$ ,  $\eta_2 = .02$ ,  $f/2 = .05$ , a cavity enhancement of unity, and a count rate of  $4.2 \times 10^4 \text{sec}^{-1}$  ( $I_o = 200$  amps), we get an estimated density of  $n = 3.3 \times 10^7 \text{cm}^{-3}$ . We can calculate the density reduction from beam divergence from Equation 3.10 for an oven aperture of .044  $\text{cm}^2$  and a distance of 31 cm, from which we can determine an oven density of  $10^{13} \text{cm}^{-3}$ . This density corresponds to a temperature just below the effusive limit for our oven. The densities which correspond to the effusive data at 210 amps are about 50% higher, and the supersonic densities are higher by a factor of 100 for 225 amps.

## 5.7 Recommendations and Conclusions

The velocity selector operates in a manner fairly consistent with theory. When selecting slow atoms, we should include an additional reduction of 50% to account for an additional reduction which we cannot now explain. A total density can be calculated to within that factor of two from the oven temperature knowing the divergence and velocity selector density reduction factors.

At the beginning of this chapter we estimated that a density of  $2.6 \times 10^4 \text{cm}^{-3}$  would give us a signal to noise ratio of five while counting 20 minutes per point. Our theory gives us a beam divergence density reduction factor for an oven aperture area of .044  $\text{cm}^2$  and a distance of 31 cm which is  $3.6 \times 10^{-6}$  (Equation 3.10). It also gives us a velocity selector density reduction factor for  $\gamma = .45$  and  $\alpha = .15$  of  $2.0 \times 10^{-3}$  (Equation 3.14). The highest oven density we can get with an effusive beam is about  $5 \times 10^{13}$  based on

our estimate of Section 5.6. Reducing this density by the reduction factors above and the additional loss of 50% we saw from the experiments, we calculate a density in the interaction region of  $1.8 \times 10^5 \text{cm}^{-3}$ , which is better than the estimate of the required density. The conclusion is that the cavity Doppler effect does not make the experiment impossible.

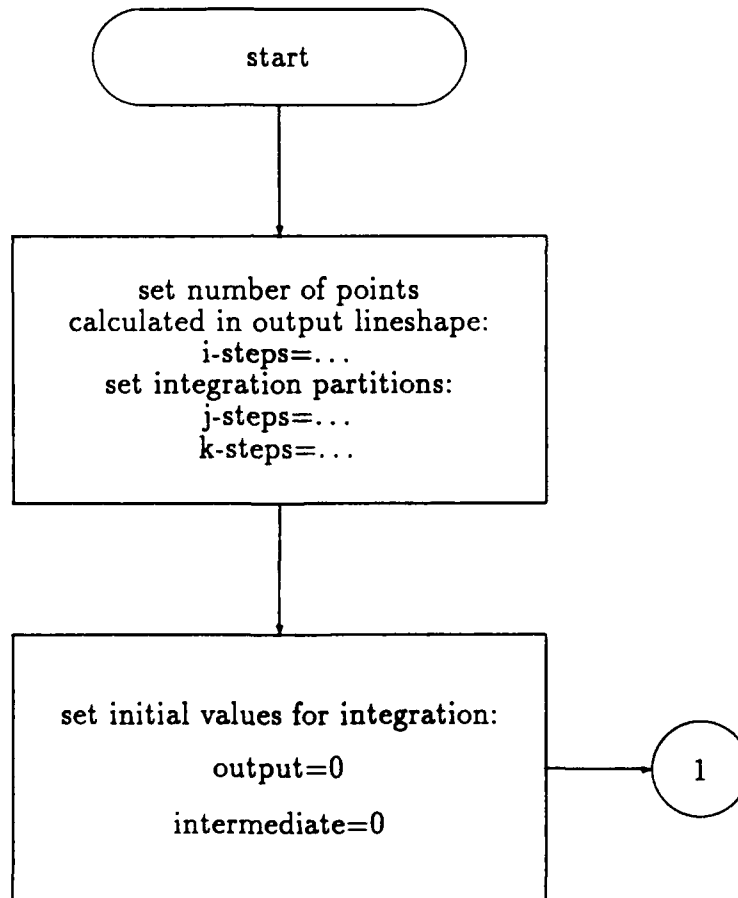
We are already planning to determine the absolute density with more accuracy, which is an important step. It would also be useful to regulate the oven current and somehow attach a thermocouple to the oven. Much work still needs to be done to neutralize the vibrations, perhaps by isolating the velocity selector and motor from the chamber. Our velocity selector design is good from the standpoint of getting good densities and an adequate velocity profile, but the misalignment problem we discovered means that we must take more care in aligning the velocity selector or change to a longer design.

The most important result of this work is that we can fairly predict the behavior of the velocity selector in future experiments and understand its limitations. Although our calculations show the cavity Doppler effect limitations can be overcome, it is at the expense of long counting times, and therefore we would want to optimize our use of the velocity selector so we do not count unnecessarily long. This problem is addressed at Appendix B for a finesse of 70 and  $f = .1$ . From that analysis, I would recommend we not build another velocity selector, but use the one we have with  $\gamma = .44$  and run the velocity selector at a speed for  $\alpha = .15$ . This would give us a contrast ratio of better than 1.2 and a minimum counting time of 30 seconds per point.

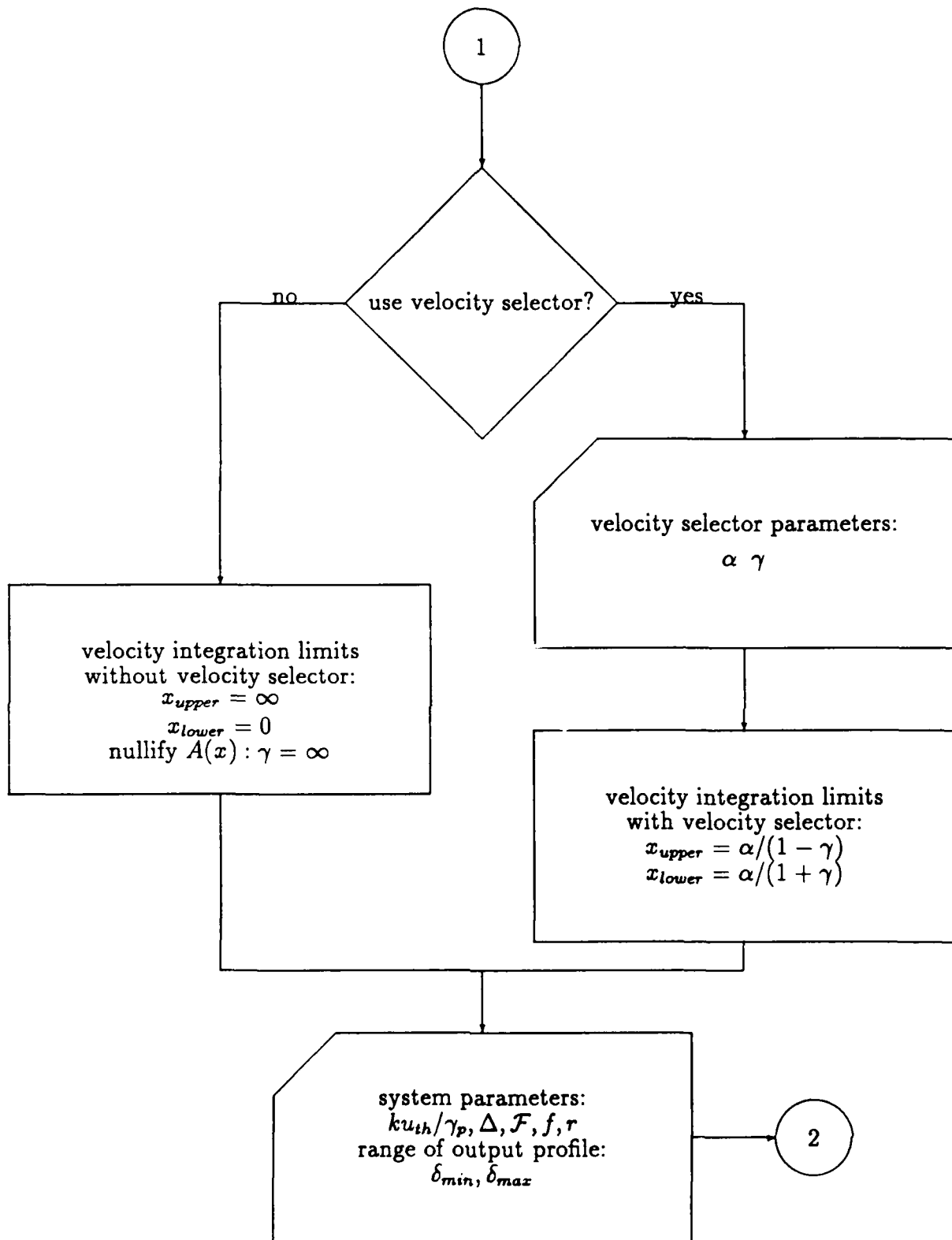
# Appendix A

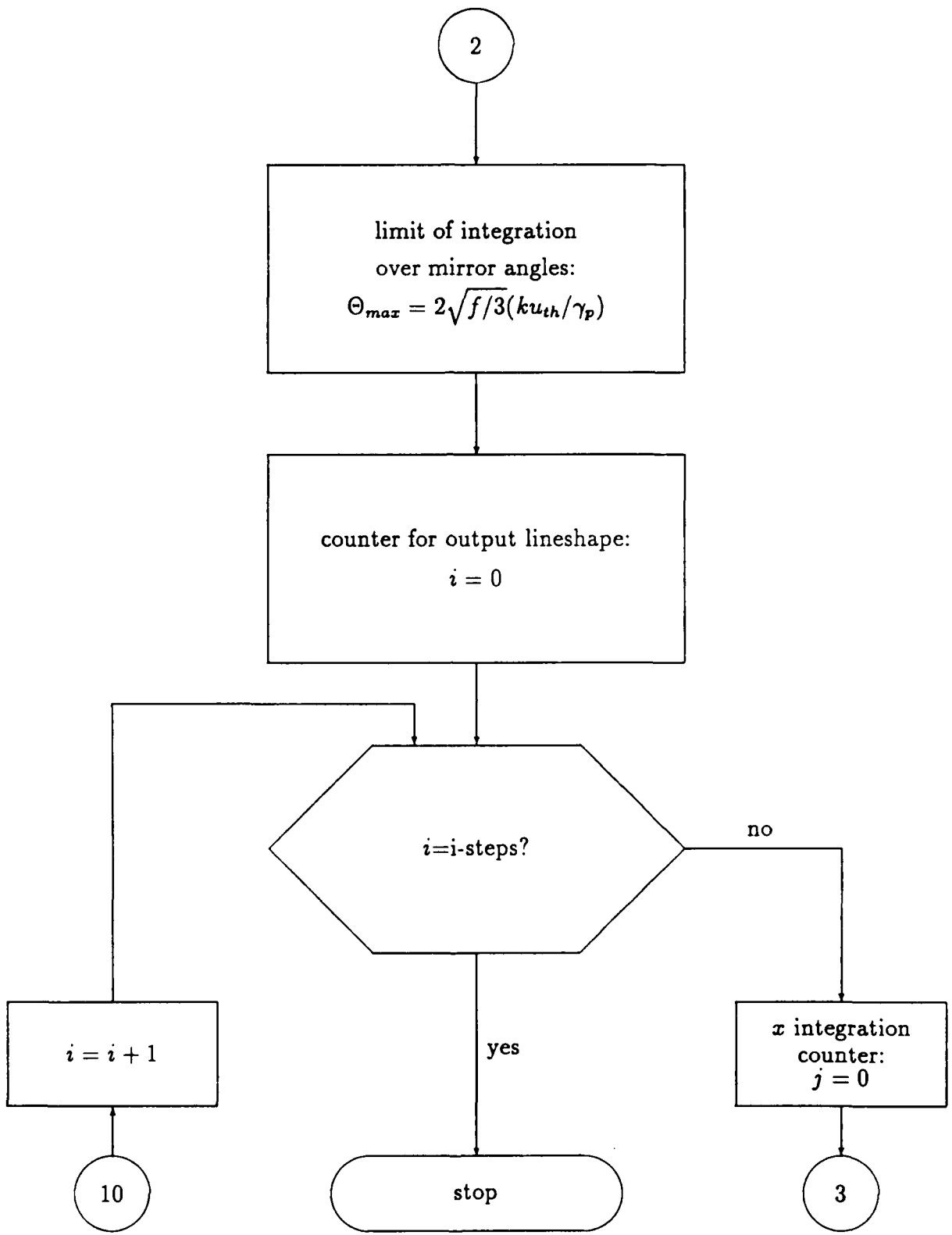
## Flowchart for Computing

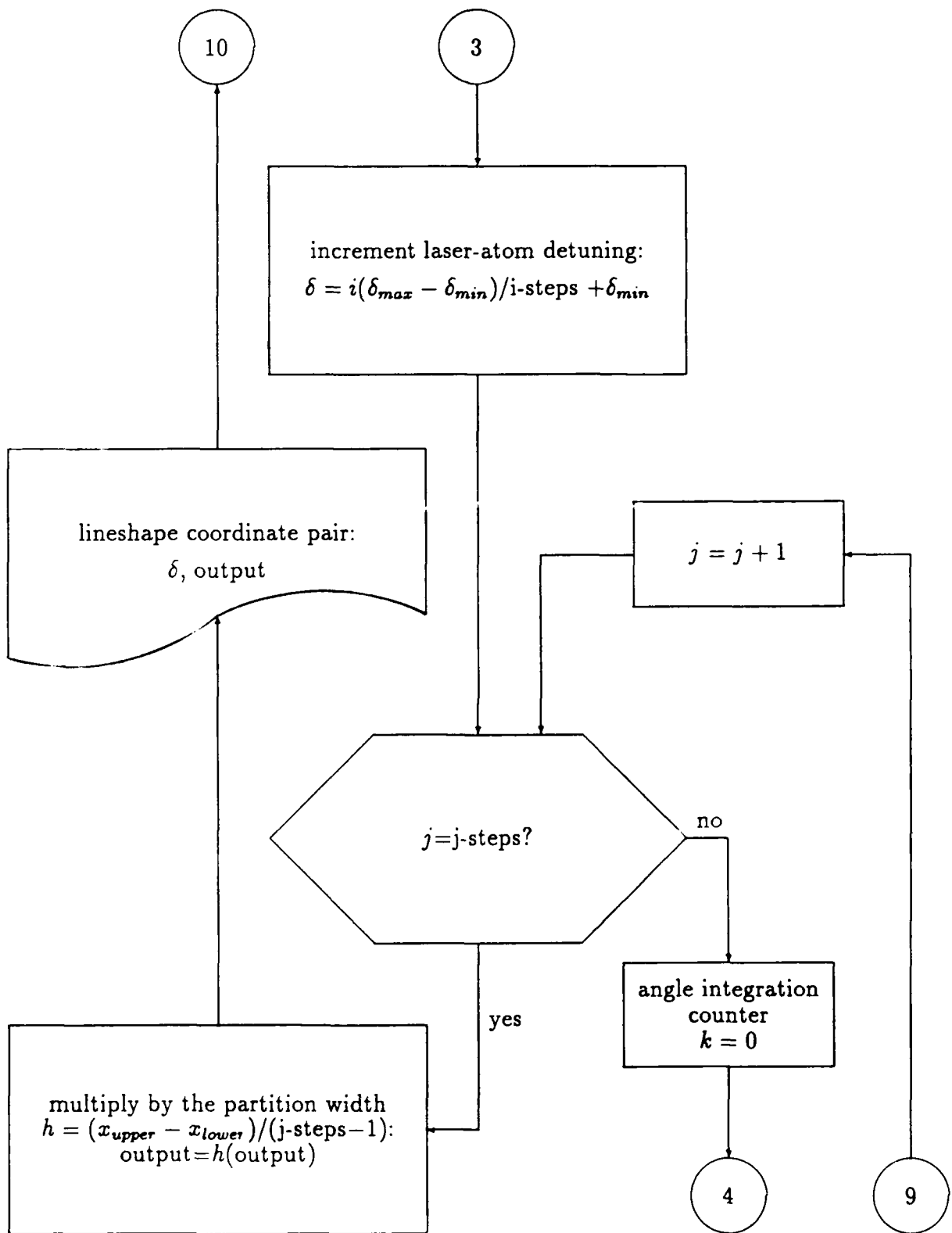
## Atom-Cavity System Lineshape<sup>1</sup>

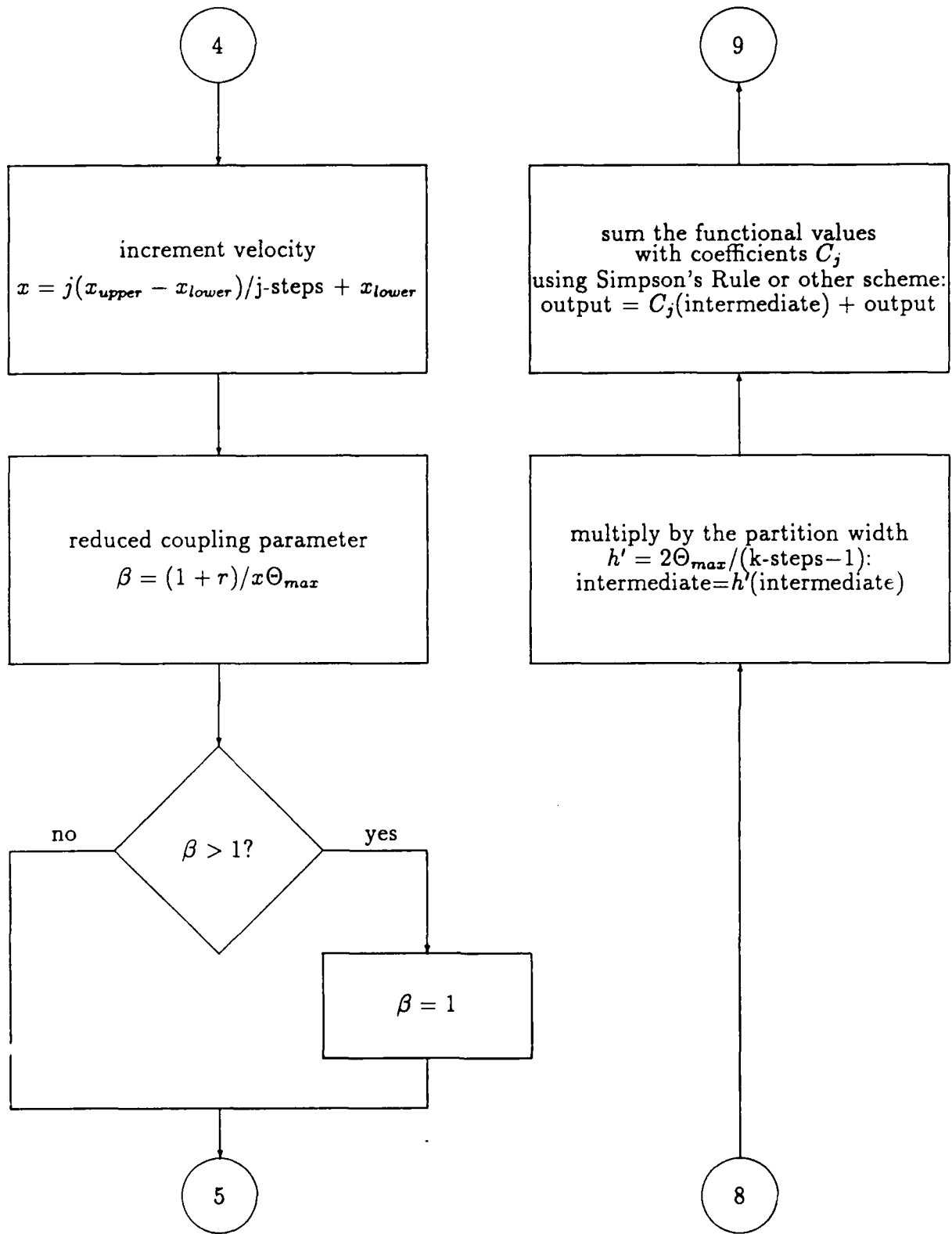


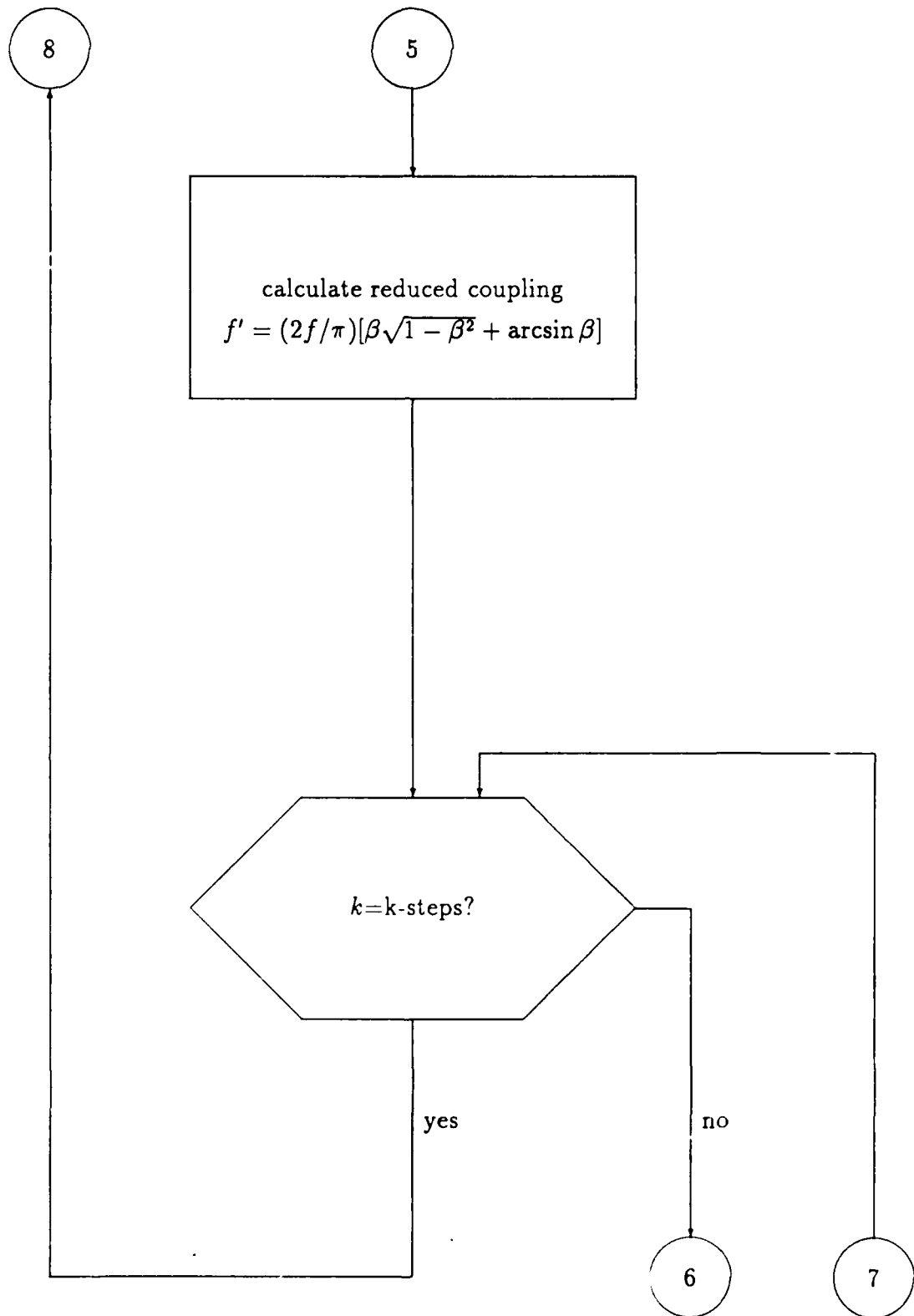
<sup>1</sup>See Section 4.4

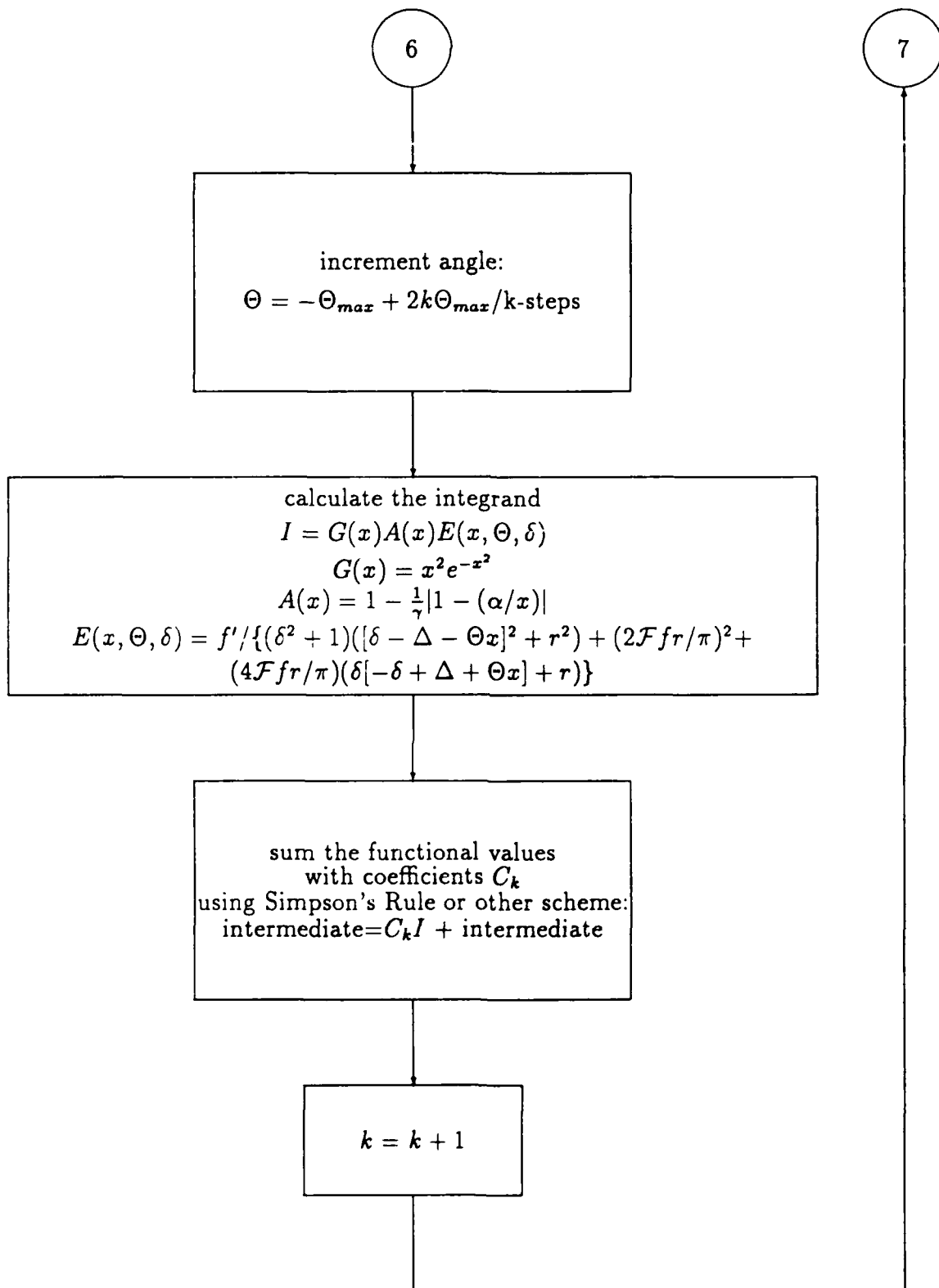












## Appendix B

# Optimization of Counting Time

Section 5.7 concludes that the atomic densities we would expect to achieve using velocity selection and counting for a “reasonable” time of twenty minutes per data point are adequate to resolve the normal mode splitting, but we have no desire to count for such a period. Collecting fifty data points would take seventeen hours! This appendix attempts to optimize the counting time assuming we have a finesse of  $\mathcal{F} = 70$  and a solid angle factor  $f = .1$ . This optimization is essentially a minimization given certain constraints and assumptions.

The method of this appendix is to determine a minimum required signal to noise ratio based on the contrast ratio as discussed in Section 4.5, and then apply Equation 5.1 to determine the counting time. Solving Equation 5.1 for the counting time per data point  $T$ , we get

$$T = \frac{X^2}{S} \left( 1 + \frac{B}{S} \right) \quad (\text{B.1})$$

where  $X$  is the minimum required signal to noise ratio,  $B$  is the background count rate, and  $S$  is the signal count rate.

Assuming the only source of data fluctuations to be statistical error, the statistical variance of the data, which is described by a Poissonian distribution, is  $\sigma^2 = (B + S)T$  [15][p. 40]. We will consider the split peaks and the local minimum between them to have signal count rates roughly calculable from Equation 5.3. The probable error of data

at these points is  $P.E. = \frac{2}{3}\sigma$  (half of the data points are within one P.E. [15][p. 46]). We will consider the data to be resolved if all data points within one probable error of the maxima have more counts than all data points within one probable error of the minimum. This is expressed mathematically by the condition

$$\frac{ST + \frac{2}{3}\sigma}{ST - \frac{2}{3}\sigma} < C.R. \quad (B.2)$$

where the contrast ratio C.R. is defined as in Section 4.5. We can then solve for the required signal to noise ratio

$$\frac{ST}{\sigma} = X > \frac{\frac{2}{3}(C.R. + 1)}{(C.R. - 1)} \quad (B.3)$$

The numbers used in this appendix for the signal count rate estimate (Equation 5.3) are the same as throughout this thesis:  $\tau = 8 \text{ nsec}$ ,  $I/I_s = .2$ ,  $V_{int} = 10^{-9} \text{ cm}^3$ ,  $\eta_1 = .3$ ,  $\eta_2 = .02$ ,  $f/2 = .05$ , and a cavity enhancement factor of fifteen. The oven density is taken to be  $5 \times 10^{13} \text{ cm}^{-3}$  which is reduced by the beam divergence reduction of  $3.6 \times 10^{-6}$  and the additional observed reduction of  $\frac{1}{2}$ .

Table B.1 shows the counting time per data point for combinations of  $\alpha$  and  $\gamma$ . Certain trends are evident that are important in selecting a good combination of these variables. For any given velocity selector speed, or  $\alpha$ , count times go up when you narrow the resolution of the velocity selector  $\gamma$  past a certain value. This is because the cavity Doppler broadening is no longer contributing in a significant way to the lineshape of the atom-cavity system, yet as the resolution is narrowed, the density is still decreasing. Past some point where the resolution gets too broad, however, the count rate also increases, because very high signal to noise ratios are then required to meet our contrast ratio criteria. Between these limits are the optimum count times.

Since the background count rate is larger than the signal count rate, the ratio  $B/S$  is critical to the counting time. If background were small compared to the signal, the signal to noise ratio  $X$  would be the more critical factor since it enters the counting time

equation squared while the signal rate would enter linearly. As it is now, however, the counting time is greatly affected by the signal size, and the estimates in the table would be grossly inaccurate for an order of magnitude error in the density estimate.

If non-statistical sources of fluctuation can be eliminated, and the estimates included here are correct, the calculations in the table are encouraging. The count times are reasonable for the velocity selector we already have with  $\gamma = .44$ . We would not gain much by redesigning it. Data that showed a contrast ratio of 1.2 would be convincing, which can be achieved by selecting at  $\alpha = .15$  (if our crude inclusion of the cavity Doppler effect is adequate). The actual count times for the experiment should be longer than the minimum, which allows us to resolve the peaks, but not to make a very precise measurement.

$\alpha$	$\gamma$	V.S. Den. Red.	$S$	C.R.	$X$	$T$
.10	.4	$4.94 \times 10^{-4}$	2.54	1.47	3.50	190
	.5	$7.48 \times 10^{-4}$	3.84	1.43	3.77	100
	.6	$1.18 \times 10^{-3}$	6.07	1.36	4.42	56
	.65	$1.52 \times 10^{-3}$	7.81	1.31	4.97	44
	.7	$2.02 \times 10^{-3}$	10.4	1.24	6.22	39
	.75	$2.82 \times 10^{-3}$	14.5	1.17	8.51	39
	.8	$4.19 \times 10^{-3}$	21.5	1.09	14.9	48
.15	.4	$1.64 \times 10^{-3}$	8.43	1.30	5.11	40
	.45	$2.01 \times 10^{-3}$	10.3	1.27	5.60	33
	.5	$2.47 \times 10^{-3}$	12.7	1.25	6.00	25
	.6	$3.85 \times 10^{-3}$	19.8	1.17	8.51	22
	.7	$6.52 \times 10^{-3}$	33.5	1.08	17.3	36
.20	.2	$1.53 \times 10^{-3}$	7.86	1.23	6.46	73
	.3	$2.50 \times 10^{-3}$	12.8	1.20	7.33	37
	.35	$3.09 \times 10^{-3}$	15.9	1.19	7.68	27
	.4	$3.79 \times 10^{-3}$	19.5	1.17	8.51	23
	.45	$4.64 \times 10^{-3}$	23.8	1.14	10.2	23
	.475	$5.13 \times 10^{-3}$	26.4	1.14	10.4	20
	.5	$5.68 \times 10^{-3}$	29.2	1.13	11.2	19
	.525	$6.30 \times 10^{-3}$	32.4	1.12	12.3	19
	.55	$7.01 \times 10^{-3}$	36.0	1.10	14.0	21
	.575	$7.82 \times 10^{-3}$	40.2	1.08	16.5	24
	.6	$8.76 \times 10^{-3}$	45.0	1.08	18.2	24
.7	$1.45 \times 10^{-2}$	74.5	1.02	61.3	120	
.25	.35	$5.87 \times 10^{-3}$	30.2	1.10	14.0	28
	.4	$7.18 \times 10^{-3}$	36.9	1.09	15.6	24
	.45	$8.75 \times 10^{-3}$	45.0	1.07	19.2	26
	.5	$1.07 \times 10^{-2}$	55.0	1.05	24.9	32
	.6	$1.62 \times 10^{-2}$	83.3	1.03	50.0	66
.30	.45	$1.45 \times 10^{-2}$	74.5	1.03	43.7	60
.35	.45	$2.19 \times 10^{-2}$	113	1.01	103	177

Table B.1: Minimum Counting Times ( $T$ ) in seconds. Columns are  $\alpha$ ,  $\gamma$ , Velocity Selector Density Reduction, signal count rate  $S$ , contrast ratio C.R., minimum signal to noise ratio  $X$ , and count time in seconds  $T$ .

# Bibliography

- [1] G. Bekefi and A.H. Barrett, *Electromagnetic Vibrations, Waves, and Radiation*, (MIT Press, Cambridge, MA, 1977)
- [2] Serge Haroche and Daniel Kleppner, "Cavity Quantum Electrodynamics", *Physics Today*, 24-30 (January 1989)
- [3] H.J. Kimble, M.G. Raizen, R.J. Thompson, R.J. Brecha, H.J. Carmichael, and Y. Shevy, "Dissipative Quantum Dynamics in Cavity Q.E.D. ", *Laser Spectroscopy IX*, 144-148 (Academic Press, Boston, 1989)
- [4] D.J. Heinzen and M.S. Feld, "Vacuum Radiative Level Shift and Spontaneous Emission Linewidth of an Atom in an Optical Resonator", *Phys. Rev. Letters* **59**, 2623-2626 (1987)
- [5] M.G. Raizen, R.J. Thompson, R.J. Brecha, H.J. Kimble, and H.J. Carmichael, "Normal-Mode Splitting and Linewidth Averaging for Two-State Atoms in an Optical Cavity", *Phys. Rev. Letters* **63**, 240-243 (1989)
- [6] Amnon Yariv, *Quantum Electronics*, (3d Ed., Wiley, New York, 1989)
- [7] J.J. Childs, M. Donovan, D.J. Heinzen, J.T. Hutton, F.W. Dalby, W.Y. Hsu, R. Glauber, and M.S. Feld, "Single Atom-Field Coupled Quantum Oscillators", *Laser Spectroscopy IX*, 153-156 (Academic Press, Boston, 1989)
- [8] M. Sargent III, M.O. Scully, and W.E. Lamb, Jr., *Laser Physics*, (Addison-Wesley, Reading, MA, 1974)

- [9] M.S. Feld, "Steady State and Transient Behavior of Two- and Three-Level Systems", *Les Houches Session XXVII 1975 / Frontiers in Laser Spectroscopy*, 206-297 (North-Holland, 1977)
- [10] J.J. Childs, D.J. Heinzen, J.T. Hutton, and M.S. Feld, "Semiclassical Analysis of Single Atom Emission in an Optical Resonator", (to be published)
- [11] R.C. Miller and P. Kusch, "Velocity Distribution in Potassium and Thallium Atomic Beams", *Phys. Rev.* **99**, 1314-1321 (1955)
- [12] A. Kantrowitz and J. Grey, "A High Intensity Source for the Molecular Beam. Part I. Theoretical", *The Rev. of Sci. Inst.* **22**, 328-337 (1951)
- [13] N.F. Ramsey, *Molecular Beams*, (Oxford University Press, Oxford, 1956)
- [14] D.J. Heinzen, J.J. Childs, J.E. Thomas, and M.S. Feld, "Enhanced and Inhibited Visible Spontaneous Emission by Atoms in a Confocal Resonator", *Phys. Rev. Letters* **58**, 1320-1323 (1987)
- [15] Philip R. Bevington, *Data Reduction and Error Analysis for the Physical Sciences*, (McGraw Hill, New York, 1969)